Target-Constrained Interference-Minimized Band Selection for Hyperspectral Target Detection

Xiaodi Shang, *Graduate Student Member, IEEE*, Meiping Song, *Member, IEEE*, Yulei Wang, *Member, IEEE*, Chunyan Yu, *Member, IEEE*, Haoyang Yu, *Member, IEEE*, Fang Li, and Chein-I Chang, *Life Fellow, IEEE*

***Abstract*— Wealthy spectral information provided by hyperspectral image (HSI) offers great benefits for many applications in hyperspectral data exploitation. However, processing such high-dimensional data volumes that may result in redundant bands due to its high interband correlation will be a challenge. For target detection and classification, this is particularly true since there may only need a relatively small number of bands that respond one particular target of interest well, while most of other bands do not. Band selection (BS) is a major dimensionality reduction technique to remove the redundant bands and selects a few bands to represent the entire image. However, how to eliminate the effect of uninteresting targets with similar spectra on detection of interesting targets is a severe issue arising in target detection for BS. This article develops a new approach called target-constrained interference-minimized BS (TCIMBS) which can be used to select band subset for specific target detection, while annihilating targets of no interest and suppressing interferers and background. Its idea is derived from target-constrained interference-minimized filter (TCIMF). By taking advantage of TCIMF, two band prioritization (BP) criteria called forward minimum variance BP (FMinV-BP) and backward maximum variance BP (BMaxV-BP) along with their three band search-based BS counterparts called sequential forward TCIMBS (SF-TCIMBS), sequential backward TCIMBS (SB-TCIMBS), and improved SB-TCIMBS (SB-TCIMBS*) are derived. The experimental results suggest that TCIMBS can improve the detection accuracy and also achieve better performance in comparison with several state-of-the-art methods.**

***Index Terms*— Band prioritization (BP), band selection (BS), hyperspectral image (HSI), target detection, target-constrained interference-minimum filter (TCIMF), virtual dimensionality (VD).**

Manuscript received June 17, 2020; accepted July 16, 2020. Date of publication August 26, 2020; date of current version June 24, 2021. This work was supported in part by the National Nature Science Foundation of China under Grant 61601077, Grant 61971082, and Grant 61890964; and in part by the Fundamental Research Funds for the Central Universities under Grant 3132019341. *(Corresponding author: Meiping Song.)*

Xiaodi Shang, Meiping Song, Yulei Wang, Chunyan Yu, Haoyang Yu, and Fang Li are with the Center for Hyperspectral Imaging in Remote Sensing (CHIRS), Information and Technology College, Dalian Maritime University, Dalian 116026, China (e-mail: shangxiaodi@qq.com; smping@163.com; 7340912@qq.com; yuchunyan1997@126.com; yuhy@dlmu.edu.cn; lifang0105@qq.com).

Chein-I Chang is with the Center for Hyperspectral Imaging in Remote Sensing (CHIRS), Information and Technology College, Dalian Maritime University, Dalian 116026, China, also with Remote Sensing Signal and Image Processing Laboratory, Department of Computer Science and Electrical Engineering, University of Maryland, Baltimore, MD 21250 USA, and also with the Department of Computer Science and Information Management, Providence University, Taichung 02912, Taiwan (e-mail: cchang@umbc.edu).

Digital Object Identifier 10.1109/TGRS.2020.3010826

NOMENCLATURE

HSI	Hyperspectral image.
BKG	Background.
DR	Dimensionality reduction.
BS	Band selection.
BP	Band prioritization.
TCIMF	Target-constrained interference-minimized filter.
TCIMBS	Target-constrained interference-minimized BS.
FMinV-BP	Forward minimum variance BP.
BMaxV-BP	Backward maximum variance BP.
SF-TCIMBS	Sequential forward TCIMBS.
SB-TCIMBS	Sequential backward TCIMBS.
SB-TCIMBS*	Improved SB-TCIMBS.
CTBS	Constrained target BS.
SF-CTBS	Sequential forward CTBS.
SB-CTBS	Sequential backward CTBS.
SCBS	Sparse constrained BS.
CSCBS	Class signature-constrained BKG suppression.
CSCBS-SFBS	CSCBS search forward BS.
CSCBS-SBBS	CSCBS search backward BS.
SDIA	Signal-decomposed and interference-annihilated.
SNR	Signal-to-noise ratio.
SBR	Signal-to-BKG ratio.
UBS	Uniform BS.
VD	Virtual dimensionality.

I. INTRODUCTION

HYPERSPECTRAL remote sensing takes advantage of the nanoscale spectral resolution provided by an imaging spectrometer to acquire a large volume of image data with very narrow and contiguous spectra so as to achieve synchronous acquisition of ground object space, radiation, and spectral information [1]–[6]. Accordingly, hyperspectral imaging has recently developed as an emerging remote sensing technique, which greatly expands conventional remote sensing's capability in revealing subtle material substances which cannot be known or by visual inspection *a priori* [7], [8]. Therefore, it has been widely used in many applications [7]–[19], which generally cannot be resolved by multispectral imaging [20].

Specifically, this article will place its main focus on a particular application in target detection via BS.

DR can retain crucial and vital information for follow-up data processing [7, Ch. 6], so that it has been widely used to reduce the high dimensional data volumes of HSI with hundreds of spectral channels. BS is one of the major DR techniques used for this purpose by removing unnecessary redundant bands or unwanted bands such as noisy bands. A major advantage of BS over other DR approaches such as component analysis-based methods and feature extraction-based techniques is that the selected bands not only contain more useful detailed data information but also keep integrity of their spectral characteristics.

Generally, BS can be performed by several different patterns. The first one is BP-based BS which prioritizes all the spectral bands in accordance with their priority scores ranked by a BP criterion such as variance [21], mutual information [22], [38], entropy [23], information divergence [24], maximum variance principal component analysis (MVPCA) [25], constrained band selection (CBS) [26], and minimum estimated abundance covariance (MEAC) [27]. This type of BS is easy to implement and widely used. Unfortunately, the prioritization of each band is based on the data information or statistics contained in the image data and has nothing to do with specific applications. The second one is band clustering/grouping-based BS [28]–[30], [34]. Such cluster-based BS approaches first divide the bands into disjoint clusters and then select the center of each cluster to form a selected band subset. The band subsets selected by the cluster-based BS approaches are strongly influenced by initial centers and parameters. The third one is greedy-based BS [31], [32] which decouples an NP-hard combination problem through greedy mountain climbing and iteratively obtains a candidate band subset. Band subset is generally found by a band search strategy such as sequential forward selection (SFS) [33] and sequential backward selection (SBS) where SFS starts with an empty set of candidates and then increments the current candidate band subset by one band at a time, while SBS starts with the full band set and then deletes one band at a time to form the current candidate band subset. The fourth one is evolution-based BS [23], which includes a variety of evolutionary computing strategies such as particle swarm optimization (PSO) [34], [35], firefly [36], and colony algorithm [37], [38].

Regarding BS developed for target detection, Yuan *et al.* [39] developed an approach, called multigraph determinantal point process (MDPP) to capture the full structure among different bands from a graph where each band is considered as a node and the edge is specified by similarity between bands. Accordingly, a path represents a possible band subset. On the other hand, Wang *et al.* [40] proposed a multiple-band selection (MBS) method, which does not require prioritizing the bands but rather selects a desired band subset for anomaly detection. Based on constrained energy minimization (CEM) developed in [41], Geng *et al.* [42] also developed an SCBS, which is convenient for solving the global optimal solution and avoids the complicated process for searching subset from total bands. Wang *et al.* [43] proposed a new BS method called minimum variance band prioritization (MinV-BP) for multiple-target detection, which minimizes the variance generated by the desired target signal to calculate the priority of each band. Despite that the above-mentioned methods can effectively select a set of bands that are sensitive to targets of interest, they do not fully consider the interference and impact of targets of no interest which have similar spectra to that of targets of interest on BS for target detection. As a matter of fact, in many real-world applications, this type of uninteresting targets and complex BKG may greatly influence detection, result in false target identification, and also create many false alarms.

This article presents a TCIMBS approach where two BP criteria and three corresponding band search-based BS methods as their counterparts are developed to select optimal band subsets for target detection. Its idea is originated from target constrained interference-minimized filter (TCIMF) [44] but its motivation is actually inspired by three different pieces of work, the signal-decomposed and interference-annihilated (SDIA) model developed in [45], CEM [41], and orthogonal subspace projection (OSP) [12], all of which are designed for target detection. In TCIMF, two types of targets are specified, the desired target matrix $\mathbf{D}$ and the undesired target matrix $\mathbf{U}$ where $\mathbf{D}$ is used for multiple target detection and $\mathbf{U}$ is used to remove the effects of undesired targets. Moreover, the SDIA model further decomposes the target matrix $\mathbf{D}$ into two target submatrices, one consisting of targets of interest, $\mathbf{D}_{\text{interest}}$ and the other comprised targets of no interest, $\mathbf{D}_{\text{no-interest}}$. Therefore, TCIMBS expands the two-component $(\mathbf{D}, \mathbf{U})$ target matrix used in TCIMF to a three-component $(\mathbf{D}_{\text{interest}}, \mathbf{D}_{\text{no-interest}}, \mathbf{U})$ target matrix as the SDIA does. Accordingly, TCIMBS can be expected to select more effective and appropriate bands for detection of specific targets of interest in $\mathbf{D}_{\text{interest}}$, while suppressing the effect of similar targets in $\mathbf{U}_{\text{unwanted}} = [\mathbf{D}_{\text{no-interest}}\ \mathbf{U}]$ on target detection at the same time.

As a summary, four main contributions of this article can be described as follows.

1) This article develops a new BS approach, TCIMBS for target detection. It extends a two-component $(\mathbf{D}, \mathbf{U})$-based TCIMF to a three-compomnet $(\mathbf{D}_{\text{interest}}, \mathbf{D}_{\text{no-interest}}, \mathbf{U})$-based TCIMBS by considering $\mathbf{U}_{\text{unwanted}} = [\mathbf{D}_{\text{no-interest}}\ \mathbf{U}]$ as an unwanted target matrix to replace the original $\mathbf{U}$ used in TCIMF as undesired target matrix. As a result, TCIMBS selects a band subset with strong ability in responding to targets of interest via further partitioning the desired target matrix $\mathbf{D}$ into targets of interest $\mathbf{D}_{\text{interest}}$ and targets of no interest, $\mathbf{D}_{\text{no-interest}}$. In this case, the targets of no interest in $\mathbf{D}_{\text{no-interest}}$ similar to targets of interest in $\mathbf{D}_{\text{interest}}$ can be considered as unwanted targets in $\mathbf{U}_{\text{unwanted}}$ to be eliminated for further improving target detectability.
2) To implement TCIMBS, two types of TCIMF-BP criteria, FMinV-BP and BMaxV-BP, are derived.

3) In correspondence to TCIMF-BP criteria, three search strategy-based BS algorithms, SF-TCIMBS, SB-TCIMBS, and the SB-TCIMBS*, are also developed as their counterparts.
4) A comprehensive study and analysis via extensive experiments is conducted to demonstrate the advantages of TCIMBS over CTBS, CSCBS, and several state-of-the-art methods.

The remainder of this article is organized as follows. Section II briefly describes original motivations and delineates significance of this article in detail. Section III introduces the basic principles of TCIMF. Section IV derives TCIMBS. Section V designs two types of criteria for prioritizing bands. Section VI provides details of the implementation process of three search strategies based on TCIMBS. Sections VII and VIII perform experiments based on the simulated data and real data, respectively, and conduct comparative analysis on the experimental results. Section IX provides some discussions of the experimental results. Finally, Section X draws some conclusions.

II. Motivations and Significance

A. Motivations

The motivation of TCIMBS was originated from combining the ideas of CEM [41], OSP [12], and TCIMF [44], all of which are available at https://www.harrisgeospatial.com/docs/tdselectmethods.html from the popular software Environment for Visualizing Images (ENVI) which is developed by L3Harris Geospatial and has been widely used for remote sensing image analysis. TCIMF combines the strengths of both CEM and OSP to enhance the target detectability. Also, according to the SDIA model in [45], the targets in $\mathbf{D}$ used in TCIMF may be made up of two types of targets: interesting targets $\mathbf{D}_{\text{interest}}$ and uninteresting targets $\mathbf{D}_{\text{no-interest}}$. In this case, a direct use of TCIMF to detect the targets of interest in $\mathbf{D}_{\text{interest}}$ may not effectively work if it does not take care of the effect resulting from uninteresting targets in $\mathbf{D}_{\text{no-interest}}$ whose signatures are similar to those of targets in $\mathbf{D}_{\text{interest}}$. This issue was investigated previously in the SDIA model [45], but unfortunately, it was designed using full band spectral information in which case all targets in $\mathbf{D}$ to be detected are assumed to have equal responses to all spectral bands. In many practical applications, this is generally not true. TCIMBS is derived by combining all the four models, CEM, OSP, TCIMF, and SDIA, to take advantages of their benefits.

On the other hand, the BS issue for target detection has been investigated in the past. Recently, an approach called CTBS was developed in [43] to select bands according to target characteristics specified by CEM. Then CTBS was later extended to HSI classification by CSCBS-based BS [46] where the concept of multiple target detection proposed in [47] was extended to multiple-class classification via linearly constrained minimum variance (LCMV) in [49]. Despite all these efforts, CTBS and CSCBS-based BS did not take advantage of $\mathbf{U}$ in TCIMF to eliminate the effect of undesired targets on target detection which inspires the work of TCIMBS.

B. Significance of TCIMBS

The significance of TCIMBS can be summarized in four aspects.

1) The first and foremost significance is exploration of interaction between the desired target matrix denoted by $\mathbf{D}$ and undesired target matrix denoted by $\mathbf{U}$. In CTBS, only a single target is considered for BS with $\mathbf{D} = \mathbf{d}$ and no undesired targets are involved, i.e., $\mathbf{U} = \emptyset$. On the other hand, CSCBS-based BS considered $\mathbf{D}$ as a multiple target matrix for BS simultaneously but also no $\mathbf{U}$ is used, i.e., $\mathbf{U} = \emptyset$. Neither CTBS nor CSCBS-based BS includes $\mathbf{U}$ as a part of BS. As a matter of fact, the similarity between target signatures in $\mathbf{D}$ and $\mathbf{U}$ plays a key factor in BS. If one desired target $\mathbf{d}$ in $\mathbf{D}$ has its signature too similar to that of an undesired target $\mathbf{u}$ in $\mathbf{U}$, eliminating $\mathbf{u}$ could have impact on reducing the detectability of $\mathbf{d}$ and vice versa. In this case, the detection of $\mathbf{d}$ may also detect $\mathbf{u}$ which may further confuse the detection of $\mathbf{d}$. Despite that the detectability of $\mathbf{d}$ can be reduced by eliminating $\mathbf{u}$, the great benefit resulting from the use of $\mathbf{u}$ is the complete elimination of its interfering effect on detection of $\mathbf{d}$. In contrast, if the signature of a desired target $\mathbf{d}$ in $\mathbf{D}$ is dissimilar to the signature of an undesired target $\mathbf{u}$ in $\mathbf{U}$, eliminating $\mathbf{u}$ could even further enhance the detectability of $\mathbf{d}$ and vice versa.
This article conducts a detailed analysis of TCIMBS by manipulating the desired targets in $\mathbf{D}$ and the undesired targets in $\mathbf{U}$ via extensive experiments performed in Sections VII and VIII where three scenarios for BS are particularly designed, namely, single-target detection with $\mathbf{D} = \mathbf{d}$ and $\mathbf{U} = \emptyset$ for CTBS, full multiple-target detection with $\mathbf{D}$ and $\mathbf{U} = \emptyset$ for CSCBS-based BS, and partial multiple target detection with a partial set of multiple targets in $\mathbf{D}$, denoted by $\mathbf{D}_{\text{interest}}$ with $\mathbf{D}_{\text{interest}} \subset \mathbf{D}$ and $\mathbf{D}_{\text{interest}} \neq \mathbf{D}$ for TCIMBS. The 3rd scenario is of particular interest. With this scenario, $\mathbf{D}$ is broken up into two target submatrices, called targets of interest, $\mathbf{D}_{\text{interest}}$ and targets of no interest, $\mathbf{D}_{\text{no-interest}}$ as $\mathbf{D} = [\mathbf{D}_{\text{interest}}\ \mathbf{D}_{\text{no-interest}}]$. In this case, we can move the uninteresting targets in $\mathbf{D}_{\text{no-interest}}$ to the original $\mathbf{U}$ to form a new augmented undesired target matrix, considered as unwanted target matrix specified by $\mathbf{U}_{\text{unwanted}} = [\mathbf{D}_{\text{no-interest}}\ \mathbf{U}]$. As a result, the original formulation of $[\mathbf{D}\ \mathbf{U}]$ used in TCIMF can be further partitioned as a three-component $(\mathbf{D}_{\text{interest}}, \mathbf{D}_{\text{no-interest}}, \mathbf{U})$-target matrix as $[\mathbf{D}\ \mathbf{U}] = [\mathbf{D}_{\text{interest}}\ \mathbf{D}_{\text{no-interest}}\ \mathbf{U}] = [\mathbf{D}_{\text{interest}}\ \mathbf{U}_{\text{unwanted}}]$ where the original $\mathbf{D}$ and $\mathbf{U}$ used in TCIMF are now replaced with $\mathbf{D} \leftarrow \mathbf{D}_{\text{interest}}$ and $\mathbf{U} \leftarrow \mathbf{U}_{\text{unwanted}} = [\mathbf{D}_{\text{no-interest}}\ \mathbf{U}]$. It is this 3rd scenario that manifests the interaction between $\mathbf{D}_{\text{interest}}$ and $\mathbf{U}_{\text{unwanted}} = [\mathbf{D}_{\text{no-interest}}\ \mathbf{U}]$. Moreover, if we let $\mathbf{D}_{\text{interest}} = \mathbf{d}$, $\mathbf{D}_{\text{no-interest}} = \emptyset$, and $\mathbf{U} = \emptyset$, which gives rise to $\mathbf{U}_{\text{unwanted}} = \emptyset$, then the 3rd scenario is reduced to the 1st scenario. On the other hand, if we let $\mathbf{D}_{\text{interest}} = \mathbf{D}$, $\mathbf{D}_{\text{no-interest}} = \emptyset$, and $\mathbf{U} = \emptyset$ which results in

$\mathbf{U}_{\text{unwanted}} = \emptyset$, then the 3rd scenario is further reduced to the 2nd scenario.

2) It is well known that BKG has a tremendous impact on target detection. The commonly used SNR is generally not applicable to hyperspectral target detection due to the fact that an HSI usually has high SNR but a severe BKG issue caused by unknown subtle material substances which can be uncovered by its very fine spectral resolution. TCIMBS is developed to particularly deal with such an issue. It takes the least-squares error (LSE) resulting from TCIMF in [44] as a BP criterion designed for TCIMBS. Most interestingly, such TCIMF-derived criteria turn out to be so-called SBR which can be actually considered as an extension to SNR where the definition and derivations of SBR are provided in Section IV. SBR is a new concept introduced into BS.
3) According to [43, Th. 1], CTBS was derived by imposing a constraint on a single target with $\mathbf{D}$ specified by a single desired target as $\mathbf{d}$. As an extension to CTBS, [46, Th. 1] was used to derive CSCBS-based BS by imposing multiple constraints on $\mathbf{D}$ consisting of desired multiple targets corresponding to multiple class means without specifying $\mathbf{U}$. This article presents a general theorem which indeed includes these theorems as special cases by imposing constraints on both $\mathbf{D}$ and $\mathbf{U}$ simultaneously. In fact, it is this theorem that provides a basis for the fundamental design criteria for TCIMBS. Specifically, all the BS criteria derived in [43] and [46] can be readily interpreted as special cases of TCIMBS criteria.
4) Last but not the least, since CEM, TCIMF, and OSP have been used by the ENVI software, it may be very likely that TCIMBS will have potential to be also included in its future software updates. With this benefit, TCIMBS can advance further development in many applications.

III. TCIMF

Suppose that $\{\mathbf{r}_i\}_{i=1}^N$ is the set of data sample vectors in an HSI, where $\mathbf{r}_i = (r_{i1}, r_{i2}, \ldots, r_{iL})^T$, $1 \le i \le N$, represents an L-dimensional sample vector, and N and L are the total number of pixels and spectral bands, respectively. In addition, let $\mathbf{D} = [\mathbf{d}_1\ \mathbf{d}_2 \ldots \mathbf{d}_p]$ be an $(L \times p)$-dimensional signature matrix of interest and denote $\mathbf{U} = [\mathbf{u}_1\ \mathbf{u}_2 \ldots \mathbf{u}_q]$ as an $(L \times q)$-dimensional undesired target signature matrix in detection. It should be noted that $\mathbf{D}$ and $\mathbf{U}$ can be either provided by *a priori* knowledge or obtained by *a posteriori* knowledge. TCIMF aims to find a target detector which can detect signal specified by the desired target signature matrix $\mathbf{D}$ and undesired target signature matrix $\mathbf{U}$ via designing a finite impulse response (FIR) filter denoted by an L-dimensional vector $\mathbf{w} = (w_1, w_2, \ldots, w_L)^T$. The filter output energy can be minimized according to the following constraint:

$$[\mathbf{D}\ \mathbf{U}]^T\mathbf{w} = \begin{bmatrix} \mathbf{1}_{p\times 1} \\ \mathbf{0}_{q\times 1} \end{bmatrix} \tag{1}$$

where $[\mathbf{D}\ \mathbf{U}]$ is defined as $[\mathbf{D}\ \mathbf{U}] = [\mathbf{d}_1\ \mathbf{d}_2 \ldots \mathbf{d}_p\ \mathbf{u}_1\ \mathbf{u}_2 \ldots \mathbf{u}_q]$ and $\mathbf{1}_{p\times 1}$ is a $p \times 1$ vector with ones in all components and $\mathbf{0}_{q\times 1}$ is a $q \times 1$ vector with zero in its components. Using (1) as a constraint, the TCIMF problem considered in [44] can be formulated as a target constrained optimization problem

$$\min_{\mathbf{w}}\{\mathbf{w}^T\mathbf{R}\mathbf{w}\} \quad \text{s.t. } [\mathbf{D}\ \mathbf{U}]^T\mathbf{w} = \begin{bmatrix} \mathbf{1}_{p\times 1} \\ \mathbf{0}_{q\times 1} \end{bmatrix} \tag{2}$$

with the optimal weight vector $\mathbf{w}^{\text{TCIMF}}$ given by

$$\mathbf{w}^{\text{TCIMF}} = \mathbf{R}^{-1}[\mathbf{D}\ \mathbf{U}]\big([\mathbf{D}\ \mathbf{U}]^T\mathbf{R}^{-1}[\mathbf{D}\ \mathbf{U}]\big)^{-1}\begin{bmatrix} \mathbf{1}_{p\times 1} \\ \mathbf{0}_{q\times 1} \end{bmatrix} \tag{3}$$

The detector TCIMF using $\mathbf{w}^{\text{TCIMF}}$ specified by (3) can be implemented as

$$\delta^{\text{TCIMF}}(\mathbf{r}) = \left(\mathbf{R}^{-1}[\mathbf{D}\ \mathbf{U}]\big([\mathbf{D}\ \mathbf{U}]^T\mathbf{R}^{-1}[\mathbf{D}\ \mathbf{U}]\big)^{-1}\begin{bmatrix} \mathbf{1}_{p\times 1} \\ \mathbf{0}_{q\times 1} \end{bmatrix}\right)^T\mathbf{r} \tag{4}$$

where $\mathbf{R} = (1/N)\sum_{i=1}^N \mathbf{r}_i\mathbf{r}_i^T$ is the sample correlation matrix. In particular, there are p targets needed to be detected by p desired target signatures, $\mathbf{d}_1, \mathbf{d}_2, \ldots, \mathbf{d}_p$ and q undesired targets needed to be annihilated using q undesired target signatures, $\mathbf{u}_1, \mathbf{u}_2, \ldots, \mathbf{u}_q$. The size of the target signature matrix, $[\mathbf{D}\ \mathbf{U}] = [\mathbf{d}_1\ \mathbf{d}_2 \ldots \mathbf{d}_p\ \mathbf{u}_1\ \mathbf{u}_2 \ldots \mathbf{u}_q]$, and the weight matrix $\mathbf{w} = (w_1, w_2, \ldots, w_L)^T$ are $L \times (p+q)$ and $L \times 1$, respectively. In order to constrain desired target and undesired target signatures, the $(p \times q)$-dimensional vector $\mathbf{c} = (c_1, c_2, \ldots, c_p, \ldots, c_q)^T$ can be specified by

$$\mathbf{c} = \begin{bmatrix} \mathbf{1}_{p\times 1} \\ \mathbf{0}_{q\times 1} \end{bmatrix} = \left(\underbrace{1, \ldots, 1}_{p}, \underbrace{0, \ldots, 0}_{q}\right)^T \tag{5}$$

Compared with the CEM [41] and OSP [12], TCIMF combines the strengths of both of them, by suppressing BKG as CEM does and annihilating the impact of undesired target signal as OSP does. Unlike CEM and OSP, which can only detect a single target at one time, TCIMF can also simultaneously detect multiple targets in the image like LCMV. Moreover, compared to LCMV, TCIMF expands constraint vector $\mathbf{1}$ to $[\mathbf{1}_{p\times 1}\ \mathbf{0}_{q\times 1}]^T$, where the component "$\mathbf{1}$" is used to constrain the particular desired target signatures, while the component "$\mathbf{0}$" is added to annihilate the undesired target signatures. Because of these two joint constraints imposed on the desired targets and undesired targets, TCIMF can improve the detection ability of the detector on the targets of interest as desired targets by imposing the constraint vector "$\mathbf{1}$" and the constraint vector "$\mathbf{0}$" on undesired targets to eliminate the influence of undesired targets on the desired targets. In the meantime, TCIMF can also minimize the interfering effects resulting from BKG and noise by inverting the sample correlation matrix $\mathbf{R}$.

IV. TCIMBS

The key feature of TCIMBS is $\min_{\mathbf{w}}\{\mathbf{w}^T\mathbf{R}\mathbf{w}\}$ in (2), referred to as minimum variance (MV) in [44]. Accordingly, replace the original $\mathbf{D}$ and $\mathbf{U}$ used in TCIMF with $\mathbf{D} \leftarrow \mathbf{D}_{\text{interest}}$ and $\mathbf{U} \leftarrow \mathbf{U}_{\text{unwanted}} = [\mathbf{D}_{\text{no-interest}}\ \mathbf{U}]$ mentioned in Section II, and then substitute (3) into (2) to yield the following MV, denoted

by $\mathrm{V}(\boldsymbol{\Omega})$ given by:

$$\begin{aligned}\mathrm{V}(\boldsymbol{\Omega}) &= \left(\mathbf{w}^{\mathrm{TCIMF}}\right)^T \mathbf{R}\mathbf{w}^{\mathrm{TCIMF}} \\ &= \left(\mathbf{R}^{-1}[\mathbf{D}\ \mathbf{U}]\left([\mathbf{D}\ \mathbf{U}]^T\mathbf{R}^{-1}[\mathbf{D}\ \mathbf{U}]\right)^{-1}\mathbf{c}\right)^T \mathbf{R} \\ &\quad \times\left(\mathbf{R}^{-1}[\mathbf{D}\ \mathbf{U}]\left([\mathbf{D}\ \mathbf{U}]^T\mathbf{R}^{-1}[\mathbf{D}\ \mathbf{U}]\right)^{-1}\mathbf{c}\right) \\ &= \left(\mathbf{c}^T\left([\mathbf{D}\ \mathbf{U}]^T\mathbf{R}^{-1}[\mathbf{D}\ \mathbf{U}]\right)^{-1}[\mathbf{D}\ \mathbf{U}]^T\right)\left(\mathbf{R}^{-1}\mathbf{R}\mathbf{R}^{-1}\right) \\ &\quad \times\left([\mathbf{D}\ \mathbf{U}]\left([\mathbf{D}\ \mathbf{U}]^T\mathbf{R}^{-1}[\mathbf{D}\ \mathbf{U}]\right)^{-1}\mathbf{c}\right) \\ &= \mathbf{c}^T\left([\mathbf{D}\ \mathbf{U}]^T\mathbf{R}^{-1}[\mathbf{D}\ \mathbf{U}]\right)^{-1}[\mathbf{D}\ \mathbf{U}]^T\mathbf{R}^{-1}[\mathbf{D}\ \mathbf{U}] \\ &\quad \times\left([\mathbf{D}\ \mathbf{U}]^T\mathbf{R}^{-1}[\mathbf{D}\ \mathbf{U}]\right)^{-1}\mathbf{c} \\ &= \mathbf{c}^T\left([\mathbf{D}\ \mathbf{U}]^T\mathbf{R}^{-1}[\mathbf{D}\ \mathbf{U}]\right)^{-1}\mathbf{c} \\ &= \mathbf{c}^T\left(\left(\mathbf{R}^{-1/2}[\mathbf{D}\ \mathbf{U}]\right)^T\left(\mathbf{R}^{-1/2}[\mathbf{D}\ \mathbf{U}]\right)\right)^{-1}\mathbf{c} \end{aligned} \tag{6}$$

It is interesting to note the role of

$$\mathbf{R}^{-1/2}[\mathbf{D}\ \mathbf{U}] = \left(\mathbf{R}^{1/2}\right)^{-1}[\mathbf{D}\ \mathbf{U}] \tag{7}$$

playing in (6). If we assume that $\mathbf{R}^{1/2} = \sum^{1/2}$ is a noise covariance matrix and $[\mathbf{D}\ \mathbf{U}]$ is only the signal of interest, we can further extend a single target to a signal matrix $[\mathbf{D}\ \mathbf{U}] = \mathbf{S}$, then (7) can be reformulated as signal-to-BKG ratio matrix (SBRM)

$$\begin{aligned}&\left(\mathbf{R}^{-1/2}[\mathbf{D}\ \mathbf{U}]\right)^T\left(\mathbf{R}^{-1/2}[\mathbf{D}\ \mathbf{U}]\right) \\ &\quad = \left(\left(\sum^{1/2}\right)^{-1}\mathbf{S}\right)^T\left(\left(\sum^{1/2}\right)^{-1}\mathbf{S}\right) \\ &\quad = \mathbf{S}^T\sum^{-1}\mathbf{S} = \mathrm{SBRM}\end{aligned} \tag{8}$$

which is a $(p+q)\times(p+q)$ matrix containing p desired signals and q undesired signals. As a special case of (8), if $[\mathbf{D}\ \mathbf{U}] = \mathbf{S}$ is reduced to a single $\mathbf{s}$ and Σ is reduced to $\sigma^2\mathbf{I}$ where $\mathbf{I}$ is an identity matrix, then (8) is reduced to $\sigma^{-2}\mathbf{s}^T\mathbf{s}$ which is exactly SNR.

By virtue of (8), the MV, $\mathrm{V}(\boldsymbol{\Omega})$ can be expressed in terms of SBRM as

$$\mathrm{V}(\boldsymbol{\Omega}) = \mathbf{c}^T\left(\mathbf{S}^T\sum^{-1}\mathbf{S}\right)^{-1}\mathbf{c} = \mathbf{c}^T(\mathrm{SBRM})^{-1}\mathbf{c} \tag{9}$$

Accordingly, minimizing (2) is equivalent to finding (6) and (9), which is also equivalent to maximizing SBRM in (8). In other words, (6) and (9) indeed the solution to (2) which maximizes SBRM as a criterion. Since $\mathrm{V}(\boldsymbol{\Omega})$ in (9) is derived by using the full band set $\boldsymbol{\Omega}$, we can make it adaptive to band subset $\boldsymbol{\Omega}_l$ which contains l bands by replacing $\boldsymbol{\Omega}$ in (9) with $\boldsymbol{\Omega}_l$ to derive $\mathrm{V}(\boldsymbol{\Omega}_l)$ for BS. As a matter of fact, in the following theorem, Theorem 1, we will prove that $\mathrm{V}(\boldsymbol{\Omega})$ with $\boldsymbol{\Omega}$ in (9) replaced with $\boldsymbol{\Omega}_l$ is monotonically decreasing as more bands are used, l is increased.

Assume that the HSI is consisted of a set of band images, $\{\mathbf{b}_l\}_{l=1}^L$. $\mathbf{b}_l$ is the lth band image represented by a column vector. $\boldsymbol{\Omega}_l = \{\mathbf{b}_1, \mathbf{b}_2, \ldots, \mathbf{b}_l\}$ is any band subset containing l bands, $1 \le l \le L$. Using the subset $\boldsymbol{\Omega}_l$ instead of the full band set $\boldsymbol{\Omega}$, we can define a new criterion according to the TCIMF error derived from (6), as follows:

$$\mathrm{V}(\boldsymbol{\Omega}_l) = \mathbf{c}^T\left([\mathbf{D}\ \mathbf{U}]_{\boldsymbol{\Omega}_l}^T\mathbf{R}_{\boldsymbol{\Omega}_l}^{-1}[\mathbf{D}\ \mathbf{U}]_{\boldsymbol{\Omega}_l}\right)^{-1}\mathbf{c} \tag{10}$$

It can be used for TCIMBS, which is the MV only using bands in the band set $\boldsymbol{\Omega}_l$. More significantly, we can prove the following theorem, which is vital to the development of TCIMBS:

$$\{\mathrm{V}(\boldsymbol{\Omega}_l)\}_{l=1}^L \tag{11}$$

is a monotonically decreasing sequence.

Theorem 1:

$$\begin{aligned}&\mathbf{c}^T\left([\mathbf{D}\ \mathbf{U}]_{\boldsymbol{\Omega}_{l+1}}^T\mathbf{R}_{\boldsymbol{\Omega}_{l+1}}^{-1}[\mathbf{D}\ \mathbf{U}]_{\boldsymbol{\Omega}_{l+1}}\right)^{-1}\mathbf{c} \\ &\qquad < \mathbf{c}^T\left([\mathbf{D}\ \mathbf{U}]_{\boldsymbol{\Omega}_l}^T\mathbf{R}_{\boldsymbol{\Omega}_l}^{-1}[\mathbf{D}\ \mathbf{U}]_{\boldsymbol{\Omega}_l}\right)^{-1}\mathbf{c}\end{aligned} \tag{12}$$

Proof: Proof of Theorem 1 is given in the Appendix.

Where $\mathbf{c}$ is a $(p+q)\times 1$-dimensional constrained vector which is independent of the subset $\boldsymbol{\Omega}_l$. The target matrices $[\mathbf{D}\ \mathbf{U}]_{\boldsymbol{\Omega}_l} = [\mathbf{d}_{\boldsymbol{\Omega}_l}^1\ \ \mathbf{d}_{\boldsymbol{\Omega}_l}^2 \ldots \mathbf{d}_{\boldsymbol{\Omega}_l}^p\ \ \mathbf{u}_{\boldsymbol{\Omega}_l}^1 \ldots \mathbf{u}_{\boldsymbol{\Omega}_l}^q]$ with $\mathbf{d}_{\boldsymbol{\Omega}_l}^j = (d_1^j, d_2^j, \ldots, d_l^j)^T$ and $\mathbf{u}_{\boldsymbol{\Omega}_l}^j = (u_1^j, u_2^j, \ldots, u_l^j)^T$, and $[\mathbf{D}\ \mathbf{U}]_{\boldsymbol{\Omega}_{l+1}} = \begin{bmatrix}\mathbf{D}_{\boldsymbol{\Omega}_l} & \mathbf{U}_{\boldsymbol{\Omega}_l} \\ \mathbf{d}_{l+1} & \mathbf{u}_{l+1}\end{bmatrix}$ with $\mathbf{d}_{l+1} = (d_{l+1}^1, d_{l+1}^2, \ldots, d_{l+1}^p)^T$ and $\mathbf{u}_{l+1} = (u_{l+1}^1, u_{l+1}^2, \ldots, u_{l+1}^q)^T$. Let $\{\mathbf{r}_{\boldsymbol{\Omega}_l}^i\}_{i=1}^N$ be the matrix composed of all data samples in the first l bands. The sample correlation matrix $\mathbf{R}$ is reformulated with the first l bands as follows:

$$\mathbf{R}_{\boldsymbol{\Omega}_l} = (1/N)\sum_{i=1}^N \mathbf{r}_{\boldsymbol{\Omega}_l}^i\left(\mathbf{r}_{\boldsymbol{\Omega}_l}^i\right)^T \tag{13}$$

V. BP by TCIMBS

One of the simplest and most direct methods for BS is to design a criterion for prioritizing each band based on the information and data characteristics of the band. Most importantly, the sequence $\{\mathrm{V}(\boldsymbol{\Omega}_l)\}_{l=1}^L$ has been proved to be monotonically decreasing. Therefore, we design two criteria for band prioritizing, called FMinV-BP and BMaxV-BP.

A. Forward Minimum Variance Band Prioritization

According to (6) obtained by full band set $\boldsymbol{\Omega}$, the variance resulting from TCIMF can be considered as the interfering effect caused by signal sources including undesired target signals and BKG signals which do not pass through the TCIMF (3). Therefore, for any band $\mathbf{b}_l$, we can define a forward BP criterion called FMinV-BP by letting $\boldsymbol{\Omega}_l$ in (10) be a single-band subset $\{\mathbf{b}_l\}$ as follows:

$$V(\mathbf{b}_l) = \mathbf{c}^T\left([\mathbf{D}\ \mathbf{U}]_{\mathbf{b}_l}^T\mathbf{R}_{\mathbf{b}_l}^{-1}[\mathbf{D}\ \mathbf{U}]_{\mathbf{b}_l}\right)^{-1}\mathbf{c} \tag{14}$$

where the band set $\boldsymbol{\Omega}_l$ in (10) is replaced with a single-band image $\mathbf{b}_l$ in (14), and the constrained vector $\mathbf{c}$ can be denoted by (5). Equation (14) measures the minimal variance of all the samples in band image $\mathbf{b}_l$ which are specified by target and undesired target signature in $[\mathbf{D}\ \mathbf{U}]_{\mathbf{b}_l}$. Specifically, the smaller the $\mathrm{V}(\mathbf{b}_l)$ is, the higher the priority of the lth band. Algorithm 1 shows the implementation process of FMinV-BP.

Algorithm 1 FMinV-BP

1. Initial condition:

According to (14), calculate the priority score for each band of hyperspectral image, $\{\mathrm{V}(\mathbf{b}_l)\}_{l=1}^{L}$.

2. Prioritize bands by $\{\mathrm{V}(\mathbf{b}_l)\}_{l=1}^{L}$ to get the final sequence of all the bands. Furthermore, the following equivalence is obtained.

$$\mathbf{b}_{l_j} \succ \mathbf{b}_{l_k} \Leftrightarrow \mathrm{V}(\mathbf{b}_{l_j}) < \mathrm{V}(\mathbf{b}_{l_k}) \tag{15}$$

where the notation "$\succ$" represents "superior to." The following is the final sequence of all the bands:

$$\mathbf{b}_{l_1} \succ \mathbf{b}_{l_2} \succ \cdots \succ \mathbf{b}_{l_L} \tag{16}$$

3. The final band subset of selected bands is obtained by the first n_{BS} bands, $\mathbf{\Omega}_{BS} = \{\mathbf{b}_{l_1}, \mathbf{b}_{l_2}, \ldots, \mathbf{b}_{l_{n_{BS}}}\}$ where n_{BS} is the number of bands to be selected.

B. Backward Maximum Variance Band Prioritization

In addition to using (14) to prioritize all bands, there is another idea, called BMaxV-BP, to prioritize the total bands. BMaxV-BP believes that if one band's removal from the full band set $\mathbf{\Omega}$ results in the largest variance of the remaining band subset $\tilde{\mathbf{\Omega}}_l = \mathbf{\Omega} - \{\mathbf{b}_l\}$, it should be most important for the target. Accordingly, BMaxV-BP removes the lth band $\mathbf{b}_l$ from the full-band set $\mathbf{\Omega}$, calculates the maximum variance of the remaining bands, $\tilde{\mathbf{\Omega}}_l$ by (17) and then prioritizes the total bands in the descending order according to $\mathrm{V}(\tilde{\mathbf{\Omega}}_l)$. A detailed implementation of BMaxV-BP is given as Algorithm 2.

$$\mathrm{V}\left(\tilde{\mathbf{\Omega}}_l\right) = \mathbf{c}^T \left([\mathbf{D}\ \mathbf{U}]_{\tilde{\mathbf{\Omega}}_l}^T \mathbf{R}_{\tilde{\mathbf{\Omega}}_l}^{-1} [\mathbf{D}\ \mathbf{U}]_{\tilde{\mathbf{\Omega}}_l}\right)^{-1} \mathbf{c}. \tag{17}$$

VI. BS BY TCIMBS

Many BS methods only consider the information characteristics or statistical information of HSI such as entropy, variance, and SNR and select a band subset to be used for different targets. Unfortunately, as shown in [43], different targets may respond to various bands quite differently. To address this issue, the two new TCIMBS-based BP criteria designed in Section V, FMinV-BP and BMaxV-BP, are used to evaluate how much information does a specific target contain in a band so as to select a band that has the strongest responsive ability and contains the most information to respond to the specific targets of interest. In this section, three various search strategies are developed to find an optimal band subset, which are SF-TCIMBS, SB-TCIMBS, and the SB-TCIMBS*.

Algorithm 2 BMaxV-BP

1. Initial condition:

According to (17), calculate the priority score for each band of hyperspectral image, $\{\mathrm{V}(\tilde{\mathbf{\Omega}}_l)\}_{l=1}^{L}$.

2. Prioritize bands by $\{\mathrm{V}(\tilde{\mathbf{\Omega}}_l)\}_{l=1}^{L}$ to get the final sequence of all the bands. Furthermore, the following equivalence is obtained.

$$\mathbf{b}_{l_j} \succ \mathbf{b}_{l_k} \Leftrightarrow \mathrm{V}(\tilde{\mathbf{\Omega}}_{l_j}) > \mathrm{V}(\tilde{\mathbf{\Omega}}_{l_k}) \tag{18}$$

where the notation "$\succ$" represents "superior to." The following is the final sequence of all the bands:

$$\mathbf{b}_{l_1} \succ \mathbf{b}_{l_2} \succ \cdots \succ \mathbf{b}_{l_L} \tag{19}$$

3. The final band subset of selected bands is obtained by the first n_{BS} bands, $\mathbf{\Omega}_{BS} = \{\mathbf{b}_{l_1}, \mathbf{b}_{l_2}, \ldots, \mathbf{b}_{l_{n_{BS}}}\}$ where n_{BS} is the number of bands to be selected.

Algorithm 3 SF-TCIMBS

1. Initial condition:

Let n_{BS} be the number of bands needed to be selected, which are determined by VD and $\mathbf{T} = [\mathbf{D}\ \mathbf{U}]$.
Find

$$\mathbf{b}_{l_1}^* = \arg\left\{\min_{\mathbf{b}_l \in \mathbf{\Omega}}\left(\mathbf{c}^T \left(\mathbf{T}_{\mathbf{b}_l}^T \mathbf{R}_{\mathbf{b}_l}^{-1} \mathbf{T}_{\mathbf{b}_l}\right)^{-1} \mathbf{c}\right)\right\} \tag{20}$$

2. Band augmentation:

$$\mathbf{b}_{l_j}^* = \arg\left\{\min_{\mathbf{b}_l \in \mathbf{\Omega}_{j-1}^c}\left(\mathbf{c}^T \left(\mathbf{T}_{\mathbf{\Omega}_{j-1} \cup \{\mathbf{b}_l\}}^T \mathbf{R}_{\mathbf{\Omega}_{j-1} \cup \{\mathbf{b}_l\}}^{-1} \mathbf{T}_{\mathbf{\Omega}_{j-1} \cup \{\mathbf{b}_l\}}\right)^{-1} \mathbf{c}\right)\right\} \tag{21}$$

where $\mathbf{\Omega}_{j-1} = \{\mathbf{b}_{l_1}, \mathbf{b}_{l_2}, \ldots, \mathbf{b}_{l_{j-1}}\}$ and $\mathbf{\Omega}_{j-1}^c = \mathbf{\Omega} - \mathbf{\Omega}_{j-1}$.

3. If $j < n_{\mathrm{BS}}$,

$$\mathbf{\Omega}_j = \{\mathbf{b}_{l_1}, \mathbf{b}_{l_2}, \ldots, \mathbf{b}_{l_j}\} = \mathbf{\Omega}_{j-1} \cup \{\mathbf{b}_{l_j}\} \tag{22}$$

and go step 2. Otherwise, BS is terminated. The final set of selected bands is given by $\mathbf{\Omega}_{BS} = \{\mathbf{b}_{l_1}, \mathbf{b}_{l_2}, \ldots, \mathbf{b}_{l_{n_{BS}}}\}$.

A. Sequential Forward TCIMBS

SF-TCIMBS is an SFS-based method to argument one single band at a time sequentially by (14) instead of prioritizing all bands as FMinV-BP does. It can be implemented as shown in Algorithm 3.

It should be noted that there are two key differences in SF-TCIMBS and FMinV-BP. The first one is that SF-TCIMBS will take the selected band set $\mathbf{\Omega}_j$ into consideration, while FMinV-BP only focuses on the band $\mathbf{b}_j$ selected to be evaluated for prioritizing. The second one is that compared to FMinV-BP which has to prioritize all bands, SF-TCIMBS will terminate as long as it reaches the required number of bands to be selected, n_{BS}.

B. Sequential Backward TCIMBS

Contrary to SF-TCIMBS, an SBS-based BS method can also be developed according to BMaxV-BP, called SB-TCIMBS, which selects the bands by (17). Starting from the full band set $\mathbf{\Omega}$, SB-TCIMBS removes one band at a time from the remaining band set which is not selected as described in Algorithm 4.

C. Improved Sequential Backward TCIMBS

The band to be removed by SB-TCIMBS will be the one which maximizes the variance of the remaining band set every

Algorithm 4 SB-TCIMBS

1. Initial condition:

Let n_{BS} be the number of bands needed to be selected, which are determined by VD, and $\mathbf{T} = [\mathbf{D}\ \mathbf{U}]$.

Find

$$\mathbf{b}_{l_1}^{*} = \arg\left\{\max_{\mathbf{b}_l \in \mathbf{\Omega}} \left(\mathbf{c}^T \left(\mathbf{T}_{\mathbf{\Omega}-\{\mathbf{b}_l\}}^T \mathbf{R}_{\mathbf{\Omega}-\{\mathbf{b}_l\}}^{-1} \mathbf{T}_{\mathbf{\Omega}-\{\mathbf{b}_l\}}\right)^{-1} \mathbf{c}\right)\right\} \tag{23}$$

2. Band Reduction:

$$\mathbf{b}_{l_j}^{*} = \arg\left\{\max_{\mathbf{b}_l \in \mathbf{\Omega}_{j-1}^{c}} \left(\mathbf{c}^T \left(\mathbf{T}_{\mathbf{\Omega}_{j-1}^{c}-\{\mathbf{b}_l\}}^T \mathbf{R}_{\mathbf{\Omega}_{j-1}^{c}-\{\mathbf{b}_l\}}^{-1} \mathbf{T}_{\mathbf{\Omega}_{j-1}^{c}-\{\mathbf{b}_l\}}\right)^{-1} \mathbf{c}\right)\right\} \tag{24}$$

where $\mathbf{\Omega}_{j-1} = \{\mathbf{b}_{l_1}, \mathbf{b}_{l_2}, \ldots, \mathbf{b}_{l_{j-1}}\}$ and $\mathbf{\Omega}_{j-1}^{c} = \mathbf{\Omega} - \mathbf{\Omega}_{j-1}$

3. If $j < n_{\mathrm{BS}}$,

$$\mathbf{\Omega}_j = \{\mathbf{b}_{l_1}, \mathbf{b}_{l_2}, \ldots, \mathbf{b}_{l_j}\} = \mathbf{\Omega}_{j-1} \cup \{\mathbf{b}_{l_j}\} \tag{25}$$

and go step 2. Otherwise, BS is terminated. The final set of selected bands is given by $\mathbf{\Omega}_{BS} = \{\mathbf{b}_{l_1}, \mathbf{b}_{l_2}, \ldots, \mathbf{b}_{l_{n_{BS}}}\}$.

time. In this case, the removed band is considered to be the one that can best characterize the targets of interest. This is reasonable, but this method does not guarantee that the set of bands made up of all the removed bands can meet the condition of MV according to TCIMF. Therefore, in this section, the SB-TCIMBS has been improved from another perspective based on the definition of TCIMF, called SB-TCIMBS*. Like SB-TCIMBS, SB-TCIMBS* also uses BMaxV-BP to select an appropriate band for each search process. SB-TCIMBS* deletes only one band at a time to make the remaining band set meet MV criterion. The process stops when the number of remaining bands reaches n_{BS}, and the remaining band set with n_{BS} bands is the optimal band subset to be selected. But the difference between SB-TCIMBS* and SB-TCIMBS is theoretically using the band selected by SB-TCIMBS* for target detection can minimize the output energy of overall target detection. Its detailed implementation is described in Algorithm 5.

Algorithm 5 SB-TCIMBS*

1. Initial condition:

Let n_{BS} be the number of bands needed to be selected, which are determined by VD.

2. Band augmentation:

Let $\mathbf{T} = [\mathbf{D}\ \mathbf{U}]$,

$$\mathbf{b}_{l_j}^{*} = \arg\left\{\min_{\mathbf{b}_l \in \mathbf{\Omega}_{j-1}^{c}} \left(\mathbf{c}^T \left(\mathbf{T}_{\mathbf{\Omega}_{j-1}^{c}-\{\mathbf{b}_l\}}^T \mathbf{R}_{\mathbf{\Omega}_{j-1}^{c}-\{\mathbf{b}_l\}}^{-1} \mathbf{T}_{\mathbf{\Omega}_{j-1}^{c}-\{\mathbf{b}_l\}}\right)^{-1} \mathbf{c}\right)\right\} \tag{26}$$

where $\mathbf{\Omega}_{j-1} = \{\mathbf{b}_{l_1}, \mathbf{b}_{l_2}, \ldots, \mathbf{b}_{l_{j-1}}\}$ and $\mathbf{\Omega}_{j-1}^{c} = \mathbf{\Omega} - \mathbf{\Omega}_{j-1}$.

3. If $j < (L - n_{\mathrm{BS}})$,

$$\mathbf{\Omega}_j = \{\mathbf{b}_{l_1}, \mathbf{b}_{l_2}, \ldots, \mathbf{b}_{l_j}\} = \mathbf{\Omega}_{j-1} \cup \{\mathbf{b}_{l_j}\} \tag{27}$$

and go step 2. Otherwise, BS is terminated. The final set of selected bands is given by $\mathbf{\Omega}_{BS} = \mathbf{\Omega}_{j-1}^{c} = \mathbf{\Omega} - \mathbf{\Omega}_{j-1} = \{\mathbf{b}_{l_1}, \mathbf{b}_{l_2}, \ldots, \mathbf{b}_{l_{n_{\mathrm{BS}}}}\}$.

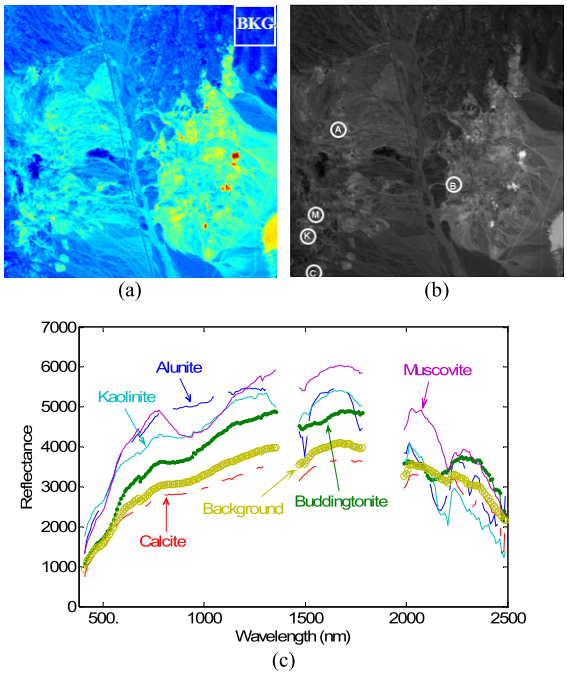

Fig. 1. (a) Cuprite AVIRIS image scene. (b) Spatial positions of five pure pixels corresponding to minerals: **A**, **B**, **C**, **K**, and **M**. (c) Five mineral reflectance spectra and BKG signature (b) which is the sample mean of the image in (a).

VII. Synthetic Image Experiments

To evaluate the effectiveness of TCIMBS, this section performs experiments on a synthetic image which was used in [7, Ch. 4]. It is target embeddedness (TE), which was particularly designed for signal detection. It was simulated from a real Cuprite image data shown in Fig. 1(a) available at the US GS website http://aviris.jpl.nasa.gov/. This scene is a 224-band image with size of 350 × 350 pixels and was collected over the Cuprite mining site, Nevada, in 1997. It is well understood mineralogically. As a result, a total of 189 bands were used for experiments where bands 1–3, 105–115, and 150–170 have been removed prior to the analysis due to water absorption and low SNR in those bands. In this particular scene, five minerals, alunite (**A**), buddingtonite (**B**), calcite (**C**), kaolinite (**K**), and muscovite (**M**) were identified by ground truth along with their spatial locations in Fig. 1(b).

Fig. 2 shows the TE simulated by 25 panels using these five mineral signatures with their appropriate abundance fractions specified the legends in Fig. 1(c). Among these 25 panels are five 4 × 4 pure-pixel panels for each row in the 1st column, five 2 × 2 pure-pixel panels for each row in the 2nd column, five 2 × 2-mixed pixel panels for each row in the 3rd column, and both the five 1 × 1 subpixel panels for each row in the 4th column and the 5th column where the mixed

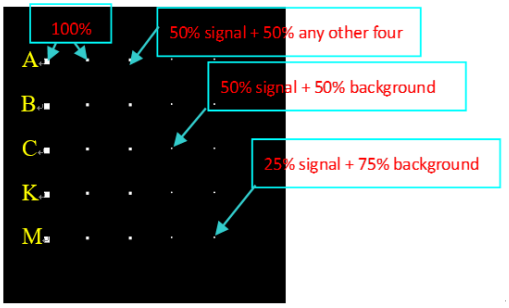

Fig. 2. Set of 25 panels simulated by **A**, **B**, **C**, **K**, and **M**.

and panel subpixels were simulated according to legends in Fig. 2. So, a total of 100 pure pixels (80 in the 1st column and 20 in the 2nd column), referred to as endmember pixels were simulated in the data by the five endmembers, **A**, **B**, **C**, **K** and **M**. An area marked by "BKG" at the upper right corner of Fig. 1(a) was selected to find its sample mean, i.e., the average of all pixel vectors within the area "BKG," denoted by **b** and plotted in Fig. 1(c), to be used to simulate the BKG for image scene in Fig. 2. The reason for this BKG selection is empirical since the selected area "BKG" seemed more homogeneous than other regions. Nevertheless, other areas can be also selected for the same purpose. This **b**-simulated image BKG was further corrupted by an additive noise to achieve a certain SNR of 20:1, which was defined as 50% signature (i.e., reflectance/radiance) divided by the standard deviation of the noise in [12].

Several state-of-the-art methods, SCBS [42], UBS, CTBS [43], and CSCBS [46], were used to conduct a comparative analysis and study. The required number of bands to be selected for TE was determined by VD [48], which was 14.

Since there are various scenarios to specify **D** and **U**, the experiments were performed from three aspects; 1) single-target detection; 2) full multiple-target detection; and 3) partial multiple-target detection to evaluate the effectiveness of TCIMBS in target detection. It should be noted that, for full multiple-target detection, **D** used by TCIMBS consists of all five targets and **U** is made up of BKG signatures extracted from the data set. In partial multiple-target detection, **D** contains more than one target of interest, and **U** consists of the remaining targets. Moreover, single-target detection is simply a special case of partial multiple-target detection. More specifically, the original desired matrix **D** used by TCIMBS is reduced to a single-target signature, $\mathbf{D} = \mathbf{d}$, and the remaining four target signatures are considered as targets of no interest to form an undesired target matrix **U**.

Qualitative and quantitative analyses were also conducted to compare the performance among various tested BS methods. Specifically, the 3-D receiver operating characteristic (ROC) developed in [7, Ch. 3] and [50]–[52] was used to calculate the area under the curve (AUC) for the three 2-D ROC curves of (P_D, P_F), (P_D, τ), and (P_F, τ) to measure the overall detection performance, target detection capability, and BKG suppression ability of a detector, respectively. That is, the higher the AUC values of (P_D, P_F) and (P_D, τ) are, the better the detection performance of the detector is. Conversely, the smaller the AUC value of (P_F, τ) is, the better the BKG suppression ability of the detector is.

A. Single-Target Detection

Four methods, UBS, SCBS, CTBS, and TCIMBS, were compared due to the fact that SCBS and CTBS are CEM-based BS methods for single-target detection. UBS was included for comparison because it is a commonly used BS method without prior knowledge and any specific application. Table I tabulates bands selected by UBS, SCBS, CTBS, and TCIMBS using each of five target signatures, **A**, **B**, **C**, **K,** and **M** as the desired target signature **d**. Fig. 3 shows the detection results of UBS, SCBS, SF-CTBS, SF-TCIMBS, SB-CTBS, SB-TCIMBS, and SB-TCIMBS* which used bands in Table I along with Table II which calculated the AUC values of three 2-D ROC curves produced by the seven methods and recorded the running times.

By visual inspection from Fig. 3, SCBS, SF-CTBS, and SB-CTBS not only detected the target of interest but also detected similar target pixels whose spectral signatures are close to the desired target signature **d**. In contrast, TCIMBS could effectively reduce the interfering effect resulting from similar targets and in the meantime, it could also improve the accuracy rate of detection. Furthermore, according to the AUC values of (P_D, P_F) in Table II, except target signatures **B** and **K**, both UBS and TCIMBS reached the same highest values, and the AUC value of SB-TCIMBS* yielded the highest values for the remaining three targets. It should be emphasized that unlike SCBS and CTBS which used CEM as the detector, the detector used by UBS and TCIMBS was TCIMF. Nevertheless, TCIMBS selected better bands for a specific target detection than UBS did. In addition, the TCIMF-detected results using SF-TCIMBS-selected bands were generally better than those using SF-CTBS-selected bands. On the other hand, the TCIMF-detected results using SB-TCIMBS*-selected bands were the best. This indicated that compared to CTBS using the same search strategies, the bands selected by TCIMBS had better characterization ability for a single target **d** and could reduce the influence of similar targets on detection of desired targets. Finally, although SCBS and UBS have advantages in time, their selected bands were not as good as those selected by TCIMBS in terms of target detection.

B. Full Multiple-Target Detection

The experiments performed in this section assumed that a full set of targets of interest was considered altogether as a whole to make up the target signature matrix **D**. In this case, the undesired target signature matrix **U** for target annihilation must be extracted from BKG where the 4×4 region at four corners of the image was extracted and their means were calculated to be used as undesired target signature to form **U**. Also, since CTBS and SCBS are designed for single-target detection, they are not applicable to multiple-target detection. So, in the experiments, only UBS, CSCBS, and TCIMBS were compared for multiple-target detection. Table III lists the

TABLE I
BAND SET SELECTED BY UBS, SCBS, CTBS, AND TCIMBS ON DETECTION OF EACH SINGLE TARGET **A, B, C, K**, AND **M** ($n_{BS} = 14$)

UBS		1	15	28	42	55	69	82	96	109	123	136	150	163	177
SCBS	**A**	134	133	105	135	132	106	131	151	153	152	58	60	107	59
	B	149	148	150	147	133	146	134	142	132	141	135	151	131	144
	C	159	157	158	172	156	160	2	18	15	1	3	16	17	67
	K	168	174	167	166	159	169	173	165	164	172	158	155	162	156
	M	1	60	58	59	61	160	161	63	62	2	152	57	4	66
SF-CTBS	**A**	58	187	60	151	54	105	50	53	152	52	106	47	134	49
	B	75	150	187	149	151	84	148	188	133	147	152	134	140	96
	C	189	172	188	171	187	170	15	169	159	173	186	160	158	18
	K	15	188	5	174	105	189	4	173	6	175	2	168	3	106
	M	34	1	35	2	33	61	36	63	32	65	37	60	30	67
SB-CTBS	**A**	187	105	106	133	134	135	104	132	103	131	54	50	58	52
	B	187	149	150	148	147	146	151	152	144	140	145	142	141	143
	C	189	187	172	173	171	170	169	168	186	188	174	167	166	159
	K	188	174	173	2	1	4	5	3	6	7	189	8	9	168
	M	1	2	4	189	3	5	6	7	8	34	35	32	37	36
SF-TCIMBS	**A**	189	34	184	82	105	47	187	62	106	175	134	50	151	48
	B	16	42	38	148	187	189	170	149	133	150	147	135	151	186
	C	34	78	124	110	62	66	105	79	74	102	189	171	172	170
	K	189	34	184	56	174	105	188	183	1	187	2	168	167	3
	M	68	48	14	3	102	33	66	36	65	35	67	34	70	29
SB-TCIMBS	**A**	105	187	106	133	134	135	104	132	103	131	162	161	163	107
	B	187	189	148	149	150	147	146	179	181	182	177	178	180	185
	C	189	187	172	171	173	170	169	168	186	188	174	167	166	159
	K	187	105	2	1	4	3	5	189	6	7	8	188	9	10
	M	1	2	4	5	3	6	189	7	8	9	10	34	35	32
SB-TCIMBS*	**A**	2	47	48	49	50	52	54	105	106	134	174	186	187	189
	B	7	15	88	105	106	133	140	148	149	150	151	182	185	187
	C	53	54	105	150	159	160	161	169	170	171	172	186	187	189
	K	1	2	3	29	36	105	134	167	168	173	174	187	188	189
	M	1	2	4	34	35	36	65	150	151	152	153	160	169	183

optimal band subsets selected by UBS, CSCBS, and TCIMBS with **D** consisting of five target signatures **A**, **B**, **C**, **K,** and **M**.

Fig. 4 shows the detection results of UBS, CSCBS-SFBS, SF-TCIMBS, CSCBS-SBBS, SB-TCIMBS, and SB-TCIMBS*. Table IV tabulates the AUC values of three 2-D ROC curves obtained from Fig. 4. From Fig. 4, the detection results of TCIMF using the band subset obtained by UBS showed that the targets were nearly embedded in BKG, especially the subpixel targets in the third column, which are barely invisible. In contrast, the detection results obtained by TCIMF using the TCIMBS-selected bands detected the targets very well and the difference between the detected targets and BKG was visibly clear. This was due to the fact that the bands selected by TCIMBS could better suppress BKG while reducing the BKG's impact on target detection. This can be also verified by the AUC value of (P_F, τ) in Table IV where the smaller the AUC value of (P_F, τ) is, the better the suppression of BKG by the detector and vice versa. In Table IV, the AUC value of (P_F, τ) produced by TCIMF using TCIMBS-selected bands was smaller than that using UBS-selected bands, which further confirms the advantage of using TCIMBS-selected bands in BKG suppression.

Furthermore, the performance of CSCBS and TCIMBS was also compared when they both used the same BS search strategies. According to the AUC values of (P_D, P_F) in Table IV, it was found that using the forward BS search method CSCBS-SFBS achieved one which was higher than SF-TCIMBS, whereas using the backward BS search method, SB-TCIMBS* also achieved the AUC value = 1, which is the same as that produced by CSCBS-SFBS. The reason is that the function of **U** in TCIMBS is to suppress the response of the similar undesired targets, while the suppression of the large BKG uses $\mathbf{R}^{-1}$. However, in the full multiple-target detection, especially in the analog image TE, **U** is selected from the simple BKG, and the spectral in **U** is very similar to that of all BKG pixels, which leads to the function of **U** being close to $\mathbf{R}^{-1}$, and the effect of **U** being minimal, making the mechanism of TCIMBS almost consistent with CSCBS. Obviously, the AUC value of (P_D, P_F) has been unable to evaluate which of the band subsets selected by these two methods is better for detection. Then, by comparing the AUC value of (P_F, τ), it can be concluded that the BKG suppression effect of SB-TCIMBS* was better than that of CSCBS-SFBS. This indicated that although **U** did not have an advantage in removing similar undesired targets, it could still reduce the influence of certain BKG pixels that $\mathbf{R}^{-1}$ cannot suppress. In conclusion, SB-TCIMBS* was the best and slightly better than CSCBS-SFBS in full multiple-target detection.

C. Partial Multiple-Target Detection

As shown in full multiple-target detection, TCIMBS had less advantages in the simulated images than in the real images to be shown in Section VIII. The reason for this is that the goal of **U** is to remove the influence of undesired targets, especially similar interfering targets in **D**, rather than to suppress the BKG. When **U** is formed by a simple signature extracted

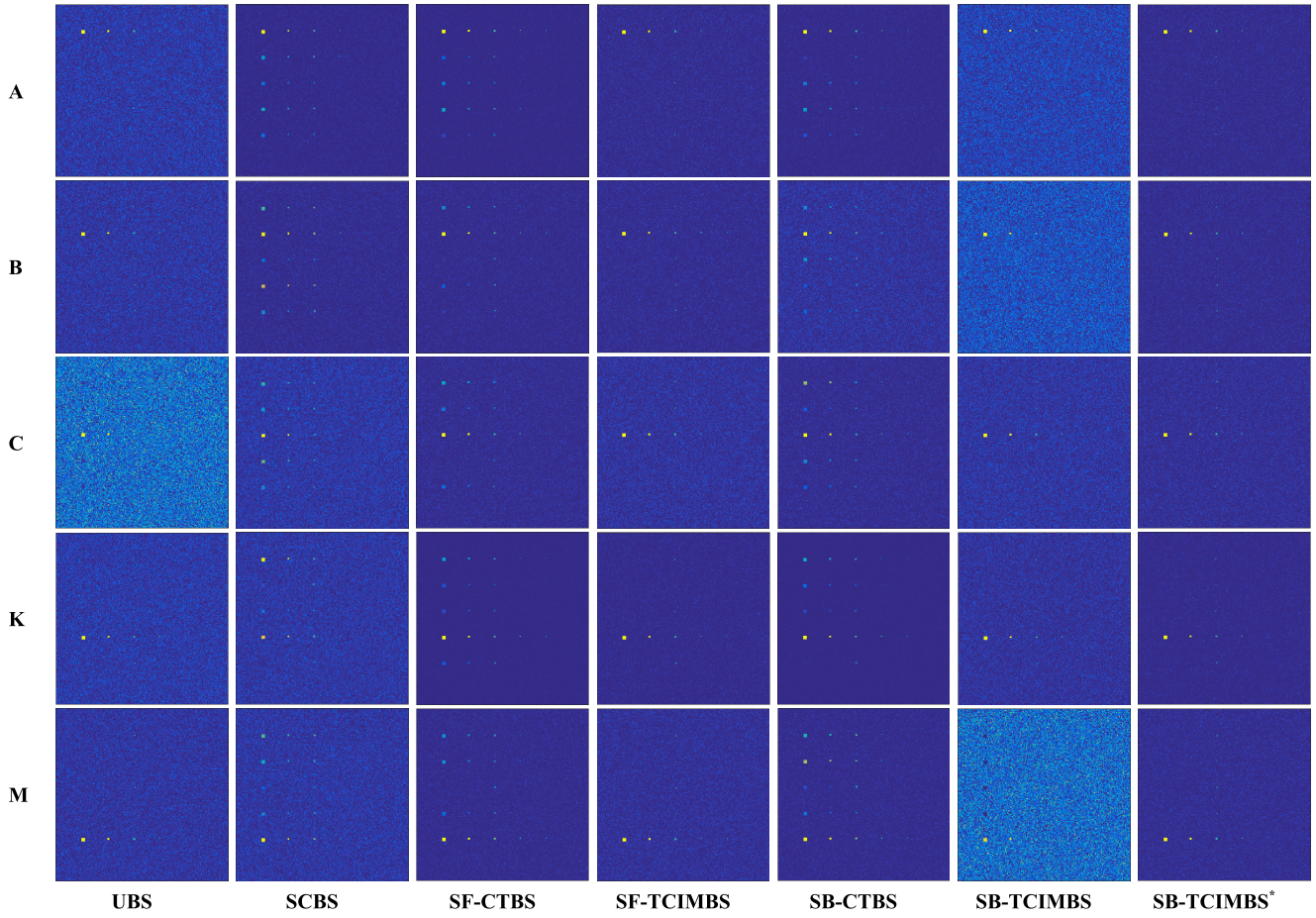

Fig. 3. CEM detection of a single target using bands selected by SCBS and CTBS as well as TCIMF detection of a single target using bands selected by UBS and TCIMBS where each single target is chosen from one of the five target signatures, **A**, **B**, **C**, **K**, and **M** in TE data.

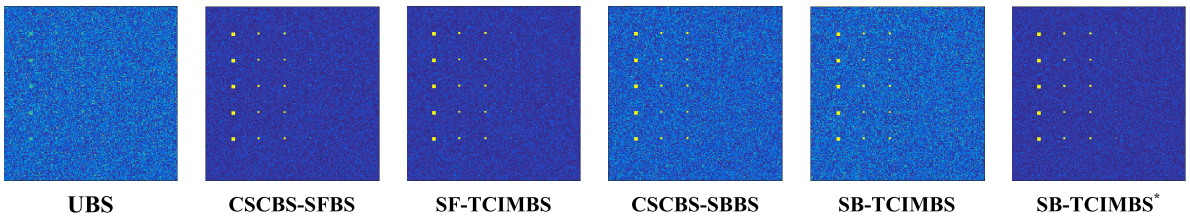

Fig. 4. LCMV detection of full multiple-target using bands selected by CSCBS and TCIMF detection of full multiple-target using bands selected by UBS and TCIMBS where full multiple-target is $\mathbf{D} = [\mathbf{A}, \mathbf{B}, \mathbf{C}, \mathbf{K}, \mathbf{M}]$ in TE data.

from BKG, its effect is very little. Therefore, partial multiple-target detection using band subsets selected by UBS, CSCBS, and TCIMBS was particularly designed to explore the removal ability of **U** in target detection.

In order to better discuss the ability of **U** to remove the similar interfering targets in **D**, the setting of the desired target matrix **D** and the undesired target matrix **U** was specifically designed and carefully selected based on the following guidelines. One is that the less the spectral similarity in the targets of interest, the better the partial-multiple target detection. The other is that the higher the spectral similarity between targets of interest and targets of no interest, the better the partial-multiple target detection. In other words, if the spectral difference between the targets of interest and targets of no interest is small, CSCBS-selected bands used for detecting interesting targets may not be effective since such similar uninteresting targets will be still considered by CSCBS as desired targets to be detected which results in false alarms. On the contrary, TCIMBS can effectively select a band subset with strong characterization ability for each target by suppressing these similar but uninteresting targets as unwanted targets so as to find better and more effective bands for each target of interest. In order to evaluate the similarity between targets, the spectral angle mapper (SAM) was used to calculate the similarity among all desired targets tabulated in Table V.

It can be seen that in the TE image, the spectral angles of targets **A** and **B**, **A** and **M**, and **C** and **K** are the

TABLE II

AUC VALUES OF (P_D, P_F), (P_D, τ), AND (P_F, τ) CALCULATED FROM THE RESULTS IN FIG. 3 AND RUNNING TIME OF EACH BS METHOD

Target	Method	AUC of (P_D, P_F)	AUC of (P_D, τ)	AUC of (P_F, τ)	Running time (s)
A	UBS	0.99998749	0.86923077	0.05120528	0.0043
	SCBS	0.99990763	0.87884615	0.01697804	0.62
	SF-CTBS	0.99994612	0.87653846	0.01311903	8.46
	SF-TCIMBS	0.99998845	0.86923077	0.02305499	10.92
	SB-CTBS	0.99996825	0.87115385	0.01654751	242.58
	SB-TCIMBS	0.99995718	0.87230769	0.07333667	349.13
	SB-TCIMBS*	0.99998845	0.86923077	0.02127183	1940.04
B	UBS	0.99998845	0.87000000	0.04507180	0.0043
	SCBS	0.99980372	0.89769231	0.02318432	0.57
	SF-CTBS	0.99996729	0.87730769	0.02020213	8.46
	SF-TCIMBS	0.99998845	0.86923077	0.02362311	10.65
	SB-CTBS	0.99994901	0.86807692	0.03778656	243.21
	SB-TCIMBS	0.99742669	0.86846154	0.10547081	348.90
	SB-TCIMBS*	0.99998845	0.86923077	0.02289088	1833.51
C	UBS	0.99188126	0.88384615	0.19842348	0.0043
	SCBS	0.99967094	0.85076923	0.04833092	0.73
	SF-CTBS	0.99992591	0.86269231	0.02421049	8.43
	SF-TCIMBS	0.99998845	0.86923077	0.03729749	10.65
	SB-CTBS	0.99981430	0.85461538	0.02459799	241.14
	SB-TCIMBS	0.99998845	0.87038462	0.04330415	348.22
	SB-TCIMBS*	0.99998845	0.86923077	0.02893131	1912.50
K	UBS	0.99998845	0.87153846	0.05221144	0.0043
	SCBS	0.99943569	0.76576923	0.04642217	0.51
	SF-CTBS	0.99996729	0.87730769	0.01061740	8.49
	SF-TCIMBS	0.99998845	0.86923077	0.01852029	10.62
	SB-CTBS	0.99996777	0.87500000	0.01046330	248.71
	SB-TCIMBS	0.99998461	0.86923077	0.03673838	346.93
	SB-TCIMBS*	0.99998845	0.86923077	0.01733827	1884.99
M	UBS	0.99998461	0.86884615	0.04227173	0.0043
	SCBS	0.99989031	0.89307692	0.04573423	0.47
	SF-CTBS	0.99994468	0.88615385	0.02088282	8.63
	SF-TCIMBS	0.99998653	0.86961538	0.03094061	10.66
	SB-CTBS	0.99985760	0.89038462	0.02089933	246.77
	SB-TCIMBS	0.95399991	0.79692308	0.19171461	346.45
	SB-TCIMBS*	0.99998845	0.86846154	0.02444464	1874.70

TABLE III

BAND SET SELECTED BY UBS, CSCBS, AND TCIMBS ON DETECTION OF FULL TARGETS $\mathbf{D} = [\mathbf{A}, \mathbf{B}, \mathbf{C}, \mathbf{K}, \mathbf{M}]$

UBS	1	15	28	42	55	69	82	96	109	123	136	150	163	177
CSCBS-SFBS	34	18	44	28	187	170	3	54	171	189	150	172	151	173
SF-TCIMBS	35	172	188	148	187	109	189	61	33	153	170	34	150	151
CSCBS-SBBS	189	187	172	173	171	170	169	168	186	188	174	167	166	159
SB-TCIMBS	189	187	172	173	171	170	169	168	186	188	174	167	166	159
SB-TCIMBS*	34	38	39	41	68	150	151	152	169	170	171	172	187	189

TABLE IV

AUC VALUES OF (P_D, P_F), (P_D, τ), AND (P_F, τ) CALCULATED FROM THE RESULTS IN FIG. 4 AND RUNNING TIME OF EACH BS METHOD

Method	AUC of (P_D, P_F)	AUC of (P_D, τ)	AUC of (P_F, τ)	Running time (s)
UBS	0.96577386	0.49384615	0.16867669	0.0043
CSCBS-SFBS	1.00000000	0.94807692	0.04678329	9.46
SF-TCIMBS	0.99999904	0.94769231	0.04759894	11.70
CSCBS-SBBS	0.99823513	0.95423077	0.14217256	252.70
SB-TCIMBS	0.99413913	0.95000000	0.16033809	375.98
SB-TCIMBS*	1.00000000	0.94769231	0.04447178	2004.27

smallest. Therefore, **D** and **U** are set to two combinations, {**A**, **C**} and {**B**, **K**, **M**} for BS and target detection of partial targets, respectively. Tables VI–IX and Figs. 5 and 6 are the results of their BS, detection, and quantitative analysis including AUC values and running time of each BS method.

Regardless of $\mathbf{D} = [\mathbf{A}, \mathbf{C}]$ or $\mathbf{D} = [\mathbf{B}, \mathbf{K}, \mathbf{M}]$, TCIMBS' constraints on the target matrix **D** and the undesired target matrix **U** in partial multiple-target detection ensure that the undesired targets can be suppressed well while the targets can be also detected. This fact was demonstrated in Tables VII and IX where the AUC values calculated by partial multiple-target

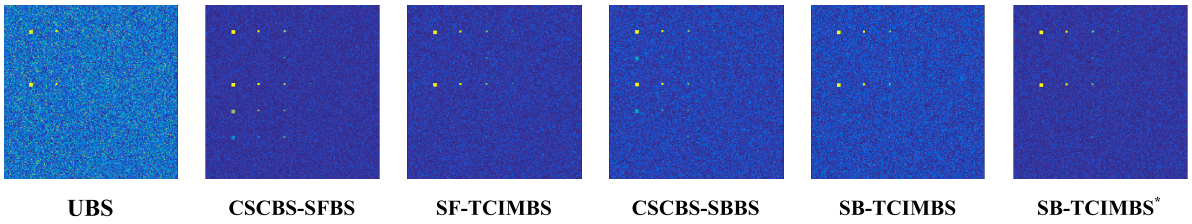

Fig. 5. LCMV detection of partial multiple-target using bands selected by CSCBS and TCIMF detection of partial multiple-target using bands selected by UBS and TCIMBS where partial multiple-target is $\mathbf{D} = [\mathbf{A}, \mathbf{C}]$ in TE data.

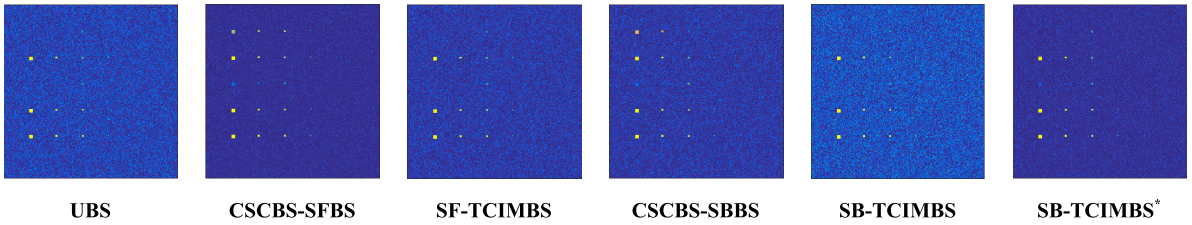

Fig. 6. LCMV detection of partial multiple-target using bands selected by CSCBS and TCIMF detection of partial multiple-target using bands selected by UBS and TCIMBS where partial multiple-target is $\mathbf{D} = [\mathbf{B}, \mathbf{K}, \mathbf{M}]$ in TE data.

TABLE V
SAM OF EACH TARGET SIGNATURE FOR TE DATA

SAM	A	B	C	K	M
A	0.00000				
B	0.03232	0.00000			
C	0.04301	0.04836	0.00000		
K	0.04025	0.05654	0.03025	0.00000	
M	0.04085	0.04582	0.05090	0.05142	0.00000

detection using the bands selected SB-TCIMBS* had the best detection performance, and its suppression effect on BKG was also relatively excellent. In addition, except the detection results of the two backward BS methods, CSCBS-SBBS and SB-TCIMBS in Table IX which were slightly worse than UBS, the results of other BS methods designed for specific targets were all better than UBS, which justified the use of the target-constrained BS method.

VIII. REAL-IMAGE EXPERIMENTS

A real-world image, hyperspectral digital imagery collection experiment (HYDICE) which is widely used in target detection has a spatial resolution of 1.56 m and contains 169 spectral bands with a size of 64 × 64. There are 15 panels divided into five types of targets, $\mathbf{p}_1$, $\mathbf{p}_2$, $\mathbf{p}_3$, $\mathbf{p}_4$, and $\mathbf{p}_5$, which are distributed on each row with three different sizes, 3 × 3, 2 × 2, and 1 × 1, respectively, shown in Fig. 7(a). Fig. 7(b) shows their precise spatial locations with the pixels in yellow (Y pixels) indicating panel pixels mixed with the BKG. In addition, there are a total of 19 panel pixels highlighted by red, which are the target pixels to focus on.

Similar to synthetic image experiments, the effectiveness of TCIMBS was also verified by single-target detection, full multiple-target detection, and partial multiple-target detection with $n_{\mathrm{BS}} = 18$ determined by VD.

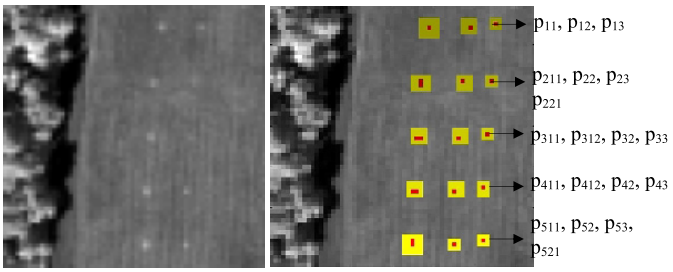

Fig. 7. (a) HYDICE panel scene. (b) Ground truth map of the 15 panels.

A. Single-Target Detection

As the same as the TE experiments, for single-target detection, each of the five target panel pixels $\mathbf{p}_1$, $\mathbf{p}_2$, $\mathbf{p}_3$, $\mathbf{p}_4$, and $\mathbf{p}_5$ was used as the desired single-target signature $\mathbf{d}$. The bands selected by UBS, SCBS, SF-CTBS, SF-TCIMBS, SB-CTBS, SB-TCIMBS, and SB-TCIMBS* are listed in Table X. The detection results using the bands in Table X along with their corresponding AUC values are also shown in Fig. 8 and Table XI.

According to the AUC values of (P_{D}, P_{F}) in Table XI, it was found that UBS had a poor detection of the panel pixels in rows 2 and 3 using target signatures $\mathbf{p}_2$ and $\mathbf{p}_3$. This is because the UBS method selected the same bands for different targets, so the selected subset of bands cannot effectively identify panel pixels in rows 2 and 3 using targets $\mathbf{p}_2$ and $\mathbf{p}_3$. Similarly, SB-TCIMBS was not effective in detecting panel pixels in rows 2, 4, and 5 using targets $\mathbf{p}_2$, $\mathbf{p}_4$, and $\mathbf{p}_5$. The reason for analysis is that SB-TCIMBS removed one band from the current band set at a time, so as to meet the maximum variance of the remaining band set. As a result, the selected band set may not be able to guarantee the MV and, thus, the best matching degree between the selected band and the desired target. In other words, the set of selected bands may not be

TABLE VI

BAND SET SELECTED BY UBS, CSCBS, AND TCIMBS ON DETECTION OF PARTIAL TARGETS $\mathbf{D} = [\mathbf{A}, \mathbf{C}]$

UBS	1	15	28	42	55	69	82	96	109	123	136	150	163	177
CSCBS-SFBS	54	78	52	79	50	172	189	170	186	105	171	53	169	55
SF-TCIMBS	34	95	126	189	48	186	62	105	170	63	106	171	61	104
CSCBS-SBBS	189	172	171	170	187	173	169	168	186	188	167	174	166	159
SB-TCIMBS	189	172	171	170	187	173	169	168	186	188	167	174	166	159
SB-TCIMBS*	48	50	52	53	54	105	106	151	161	170	171	172	186	189

TABLE VII

AUC VALUES OF (P_D, P_F), (P_D, τ), AND (P_F, τ) CALCULATED FROM THE RESULTS IN FIG. 5 AND RUNNING TIME OF EACH BS METHOD

Method	AUC of (P_D, P_F)	AUC of (P_D, τ)	AUC of (P_F, τ)	Running time (s)
UBS(TCIMF)	0.98927307	0.90307692	0.21615500	0.004278
CSCBS-SFBS	0.99988061	0.90730769	0.03973165	10.70
SF-TCIMBS	0.99998508	0.88807692	0.04730400	10.99
CSCBS-SBBS	0.99985173	0.89307692	0.06808526	276.21
SB-TCIMBS	0.99980504	0.89038462	0.08231952	361.87
SB-TCIMBS*	0.99998556	0.88769231	0.04287399	1943.62

TABLE VIII

BAND SET SELECTED BY UBS, CSCBS, AND TCIMBS ON DETECTION OF PARTIAL TARGETS $\mathbf{D} = [\mathbf{B}, \mathbf{K}, \mathbf{M}]$

UBS	1	15	28	42	55	69	82	96	109	123	136	150	163	177
CSCBS-SFBS	34	46	137	39	37	152	1	154	105	106	2	162	187	161
SF-TCIMBS	36	18	42	44	79	50	78	60	48	173	106	148	133	1
CSCBS-SBBS	187	105	106	133	135	134	189	132	131	104	161	162	163	164
SB-TCIMBS	187	105	106	133	134	135	132	104	131	162	161	103	163	164
SB-TCIMBS*	1	105	106	131	133	134	135	149	150	161	162	163	165	187

TABLE IX

AUC VALUES OF (P_D, P_F), (P_D, τ), AND (P_F, τ) CALCULATED FROM THE RESULTS IN FIG. 6 AND RUNNING TIME OF EACH BS METHOD

Method	AUC of (P_D, P_F)	AUC of (P_D, τ)	AUC of (P_F, τ)	Running time (s)
UBS(TCIMF)	0.99990510	0.90884615	0.07404364	0.004278
CSCBS-SFBS	0.99992678	0.91846154	0.02737037	10.50
SF-TCIMBS	0.99998555	0.90615385	0.05296002	10.83
CSCBS-SBBS	0.99641561	0.89807692	0.04997971	275.78
SB-TCIMBS	0.99890893	0.90923077	0.10732954	355.35
SB-TCIMBS*	0.99998699	0.90653846	0.03146836	1914.49

the most representative for the targets to be detected. This was why its improved method SB-TCIMBS* was proposed. SB-TCIMBS* guaranteed the MV of the remaining bands while removing redundant bands, so it could retain enough information to characterize the targets of interest. It turned out that the target detection results using the band set selected by SB-TCIMBS* was the best.

In general, when a similar target has a certain degree of similarity to the interesting target to be detected, SCBS and CTBS can hardly remove the information of such a similar target, leading to obvious false alarms. By taking advantage of **U**, TCIMBS performed better than SCBS and CTBS in suppressing these similar targets. From the AUC value of (P_D, P_F) for each target, most of the AUC values of using UBS-selected bands were relatively low, while using TCIMBS-selected bands always yielded higher values. In particular, TCIMF using SB-TCIMBS*-selected bands always produced the maximum AUC values. These demonstrated that TCIMBS was a very effective BS for specific single-target detection.

B. Full Multiple-Target Detection

According to the HYDICE scene, in addition to the five types of target panel pixels, there are also four types of substances in BKG, namely, grass, road, forest, and interferences in a large area. Therefore, for each BKG signature, the spectra of 9 pixels were extracted to calculate the average spectra as its signature, and then these average spectra of the four BKG signatures were used to form the undesired target matrix **U**.

Following the same experiments conducted for TE, the bands selected by UBS, CSCBS, and TCIMBS are listed in Table XII. The detection results using the bands in Table XII along with their corresponding AUC values are also shown in Fig. 9 and Table XIII, respectively. The detection results in Fig. 9 show that all the BS methods could detect the target pixels well, but the bands selected by UBS, CSCBS-SBBS, and SB-TCIMBS were not effective in suppressing BKG as the other three BS methods. Three conclusions can be drawn from the quantitative analysis of the AUC values of (P_D, P_F). First, CSCBS-SFBS had the lowest value. Second, TCIMBS had higher values than that produced by CSCBS in both forward

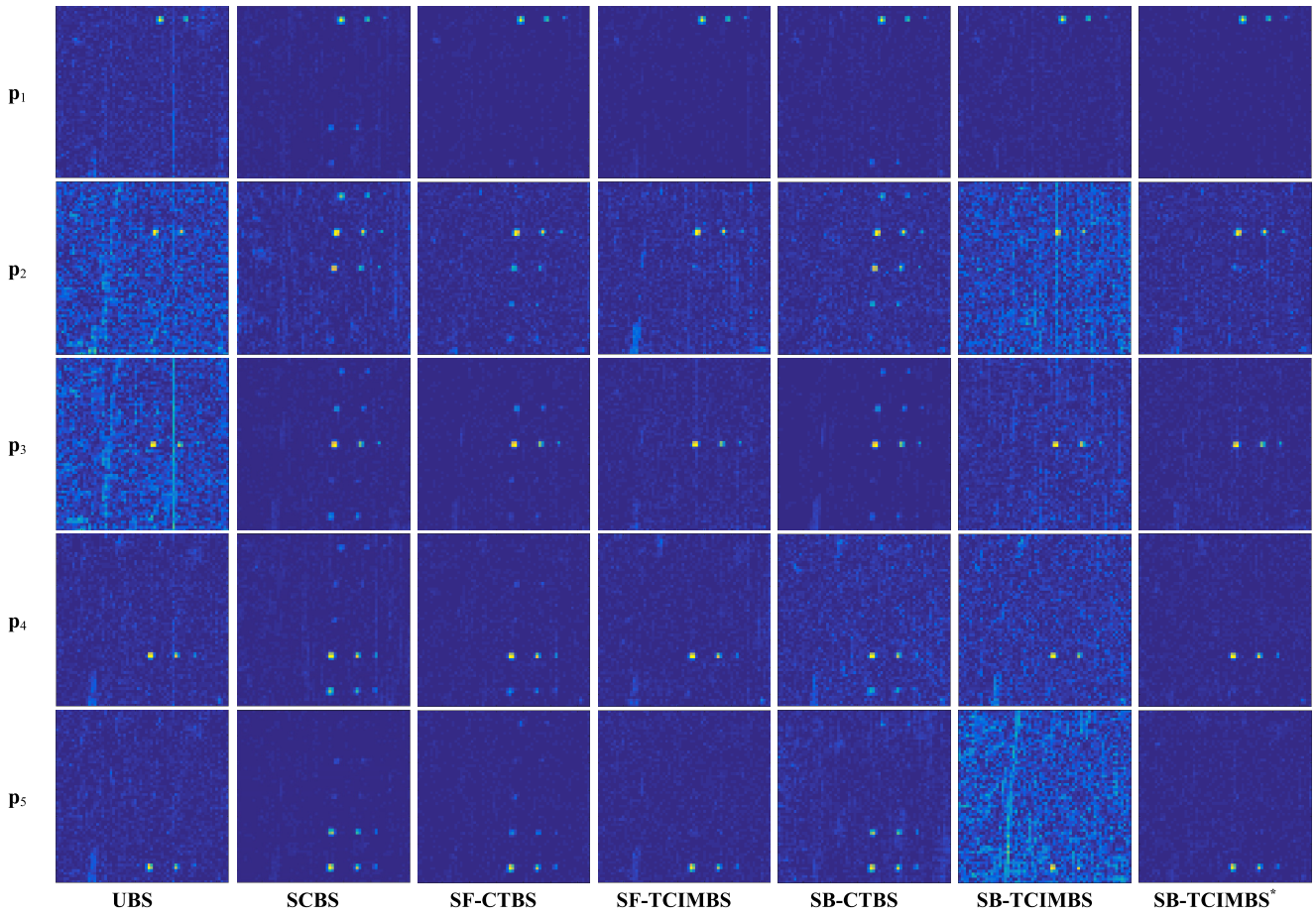

Fig. 8. CEM detection of a single target using bands selected by SCBS and CTBS as well as TCIMF detection of a single target using bands selected by UBS and TCIMBS where each single target is chosen from one of the five target signatures, $\mathbf{p}_1$, $\mathbf{p}_2$, $\mathbf{p}_3$, $\mathbf{p}_4$, and $\mathbf{p}_5$ in HYDICE data.

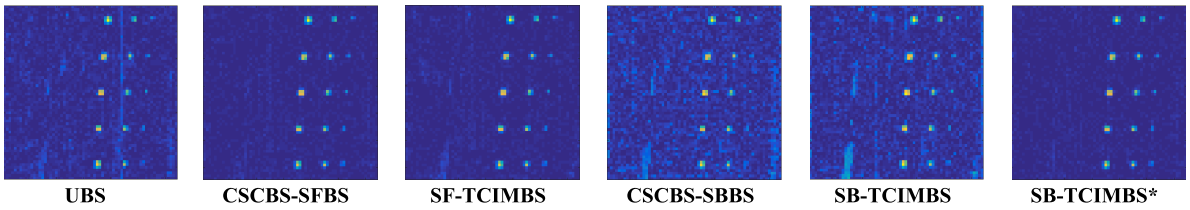

Fig. 9. LCMV detection of full multiple-target using bands selected by CSCBS and TCIMF detection of full multiple-target using bands selected by UBS and TCIMBS where full multiple-target is $\mathbf{D} = [\mathbf{p}_1, \mathbf{p}_2, \mathbf{p}_3, \mathbf{p}_4, \mathbf{p}_5]$ in HYDICE data.

and backward search manners. Third, the SB-TCIMBS* had the highest AUC value. Since the BKG of the HYDICE image is more complicated than that of the simulated TE image with a simple Gaussian noise BKG, $\mathbf{R}^{-1}$ could not suppress as it did for TE image data. In summary, using bands selected by TCIMBS for full target detection of real images could improve the detection performance.

C. Partial Multiple-Target Detection

In analogy with Table V, Table XIV calculated SAM values among five target signatures, $\mathbf{p}_1$, $\mathbf{p}_2$, $\mathbf{p}_3$, $\mathbf{p}_4$, and $\mathbf{p}_5$. As can be seen from Table XIV, the SAM values of target signatures $\mathbf{p}_1$ and $\mathbf{p}_2$, $\mathbf{p}_2$ and $\mathbf{p}_3$, $\mathbf{p}_4$ and $\mathbf{p}_5$ were the smallest. This implies that $\{\mathbf{p}_1, \mathbf{p}_2\}$ were very similar, so are $\{\mathbf{p}_2, \mathbf{p}_3\}$ and $\{\mathbf{p}_4, \mathbf{p}_5\}$. Therefore, $\{\mathbf{p}_1, \mathbf{p}_3, \mathbf{p}_4\}$ and $\{\mathbf{p}_2, \mathbf{p}_5\}$ were used as $\mathbf{D}$ and $\mathbf{U}$ for BS. Table XV lists the bands selected by UBS, CSCBS, and TCIMBS. Fig. 10 shows the target detection results of various methods. Their AUC values and running time are tabulated in Table XVI where the TCIMF-detected results using the bands selected by SB-TCIMBS were the worst and the TCIMF-detected results using bands selected by UBS were also poor. In comparison with CSCBS and TCIMBS, the forward BS method SF-TCIMBS selected better bands than CSCBS-SFBS did and the backward BS method SB-TCIMBS* was significantly better than CSCBS-SBBS in terms of selecting effective bands. On the whole, SB-TCIMBS* selected the best band subset for TCIMF detection.

TABLE X
BAND SET SELECTED BY UBS, SCBS, CTBS, AND TCIMBS ON DETECTION OF EACH SINGLE TARGET $\mathbf{p}_1$, $\mathbf{p}_2$, $\mathbf{p}_3$, $\mathbf{p}_4$, AND $\mathbf{p}_5$ ($n_{BS} = 18$)

UBS		1	10	20	29	39	48	57	67	76	86	95	104	114	123	132	142	151	161
	$\mathbf{p}_1$	105	111	112	24	104	57	67	66	28	53	49	39	103	11	79	17	25	106
	$\mathbf{p}_2$	33	99	115	69	82	90	27	26	52	100	53	67	19	57	49	58	2	83
SCBS	$\mathbf{p}_3$	45	51	46	50	44	52	47	43	35	49	19	5	34	17	15	111	36	18
	$\mathbf{p}_4$	115	114	63	61	102	103	80	65	96	33	56	57	51	69	64	25	104	32
	$\mathbf{p}_5$	25	28	24	114	26	27	115	57	61	17	89	14	38	23	39	11	56	67
	$\mathbf{p}_1$	169	127	122	105	112	149	130	116	128	123	148	17	22	2	106	109	142	132
	$\mathbf{p}_2$	122	128	133	154	143	137	142	148	153	11	27	19	6	138	46	49	42	129
SF-CTBS	$\mathbf{p}_3$	122	126	53	41	118	111	15	52	45	51	38	107	44	5	49	26	37	98
	$\mathbf{p}_4$	123	166	50	128	158	101	152	141	149	46	153	25	134	9	38	112	104	140
	$\mathbf{p}_5$	122	49	25	17	39	154	136	28	153	18	27	38	52	132	155	26	151	14
	$\mathbf{p}_1$	109	110	111	112	122	113	132	137	138	140	123	139	108	114	136	142	141	120
	$\mathbf{p}_2$	133	129	143	144	118	44	46	47	45	43	115	78	154	153	142	33	35	32
SB-CTBS	$\mathbf{p}_3$	123	45	44	46	47	43	51	52	50	49	53	54	55	56	57	48	70	39
	$\mathbf{p}_4$	158	152	154	155	153	63	156	151	150	149	159	148	147	157	161	163	166	165
	$\mathbf{p}_5$	61	62	73	67	124	58	94	114	27	28	25	26	24	113	136	23	21	29
	$\mathbf{p}_1$	122	144	154	120	119	71	126	142	79	97	128	113	106	70	58	112	117	75
	$\mathbf{p}_2$	122	128	124	163	46	169	48	154	151	50	120	113	115	42	49	142	133	107
SF-TCIMBS	$\mathbf{p}_3$	122	169	154	168	167	126	52	40	98	45	49	86	42	46	129	156	26	19
	$\mathbf{p}_4$	169	51	154	127	129	119	152	97	56	156	133	42	113	106	122	26	36	143
	$\mathbf{p}_5$	122	150	140	126	111	71	148	151	38	131	27	14	25	132	156	106	136	152
	$\mathbf{p}_1$	109	110	111	112	113	122	132	137	138	140	123	139	108	114	136	142	141	120
	$\mathbf{p}_2$	133	45	46	47	44	43	42	49	78	41	39	40	38	37	48	36	50	154
SB-TCIMBS	$\mathbf{p}_3$	123	45	44	46	47	43	42	49	41	39	38	40	37	36	48	50	70	35
	$\mathbf{p}_4$	61	62	152	158	155	154	153	156	151	150	149	159	157	148	147	161	166	165
	$\mathbf{p}_5$	61	62	73	67	58	27	28	25	114	26	24	136	23	113	94	21	29	22
	$\mathbf{p}_1$	17	28	39	49	51	54	55	70	90	93	106	110	111	116	128	132	140	148
	$\mathbf{p}_2$	19	27	38	46	50	71	82	95	97	98	101	113	115	118	123	129	133	142
SB-TCIMBS*	$\mathbf{p}_3$	27	35	38	45	46	50	52	54	56	88	98	99	109	113	123	129	133	154
	$\mathbf{p}_4$	18	26	27	33	38	54	61	63	89	98	105	112	138	143	149	152	155	156
	$\mathbf{p}_5$	17	27	28	38	52	57	61	63	78	82	89	94	106	114	122	142	151	156

Similarly, we swapped $\mathbf{D}$ and $\mathbf{U}$ as $\mathbf{D} = [\mathbf{p}_2, \mathbf{p}_5]$ and $\mathbf{U} = [\mathbf{p}_1, \mathbf{p}_3, \mathbf{p}_4]$. Table XVII lists the bands selected by UBS, CSCBS, and TCIMBS. Fig. 11 shows the detection results of various BS methods along with their AUC values and running time tabulated in Table XVIII. The TCIMF-detected results of UBS were obviously worse than those using bands selected by CSCBS and TCIMBS which are specifically designed for desired targets to be detected. However, running time of UBS is least. In general, SB-TCIMBS* was the best BS method since band set selected by SB-TCIMBS* can perform well in target detection and has excellent ability in suppressing BKG.

IX. DISCUSSION

Five concluding remarks are noteworthy.

1) Since UBS has been widely used in BS and also has its advantage of no prior knowledge required, UBS was compared to our proposed TCIMBS. The experimental results demonstrated that with the same detector used to perform target detection, SF-TCIMBS and SB-TCIMBS* performed better than UBS in terms of the AUC value of (P_D, P_F) regardless of single-target detection, full multiple-target detection, and partial multiple-target detection. This evidence shows that different targets require different sets of bands to be detected well and the same set of bands selected by UBS could only work well to some extent.
2) TCIMBS combines the advantages of both CTBS and CSCBS to select better band subsets to perform target detection well. This is because TCIMBS moves the similar targets of no interest $\mathbf{D}_{\text{no-interest}}$ in $\mathbf{D}$ to form an unwanted target matrix $\mathbf{U}_{\text{unwanted}}$ for eliminating their interfering effects on targets to be detected. The experimental results demonstrated that TCIMBS had good consistency and robustness compared with other BS methods, especially in partial multiple-target detection.
3) The selection of $\mathbf{U}$ in TCIMBS is crucial since it has direct impact on detection performance. Through the results of single-target detection and partial multiple-target detection, TCIMBS could select more effective bands when $\mathbf{U}$ is composed of similar targets of no interest in $\mathbf{D}$ which have significant impact on target detection. When the full targets are detected, there are no similar targets to be used to construct $\mathbf{U}$ in which case $\mathbf{U}$ must be formed by BKG signatures. However, BKG is so complicated that finding appropriate BKG signatures used for BKG suppression will be very challenging as demonstrated in TE and HYDICE experiments.
4) The running time(s) of various BS methods were documented for the time complexity. The used computer environment was Intel i7-6700 3.4-HZ base frequency CPU and 16-GB 2133-MHz memory. All experiments were implemented using MATLAB with version 2015b. As shown in the Tables II and XI for single-target detection, UBS required the least time, followed by SCBS and CTBS, and finally TCIMBS,

TABLE XI

AUC VALUES OF (P_D, P_F), (P_D, τ), AND (P_F, τ) CALCULATED FROM THE RESULTS IN FIG. 8 AND RUNNING TIME OF EACH BS METHOD

Target	Method	AUC of (P_D, P_F)	AUC of (P_D, τ)	AUC of (P_F, τ)	Running time (s)
$\mathbf{p}_1$	**UBS**	0.99902272	0.55833333	0.02770706	0.000566
	SCBS	0.99918560	0.57500000	0.01302590	0.38
	SF-CTBS	0.99918560	0.57833333	0.01017469	0.65
	SF-TCIMBS	0.99918560	0.56833333	0.01109822	0.91
	SB-CTBS	0.99918560	0.56166667	0.01368800	27.73
	SB-TCIMBS	0.99918560	0.56166667	0.01501710	44.42
	SB-TCIMBS*	0.99918560	0.57166667	0.00991571	164.14
$\mathbf{p}_2$	**UBS**	0.93132942	0.69250000	0.07828690	0.000566
	SCBS	0.99914467	0.80250000	0.03138807	0.39
	SF-CTBS	0.99954179	0.79000000	0.02500000	0.62
	SF-TCIMBS	0.99972507	0.78250000	0.03098485	0.90
	SB-CTBS	0.99926686	0.81250000	0.03097507	27.67
	SB-TCIMBS	0.96465665	0.66750000	0.07936950	44.27
	SB-TCIMBS*	0.99981672	0.79000000	0.02803519	164.50
$\mathbf{p}_3$	**UBS**	0.99828935	0.76500000	0.08005132	0.000566
	SCBS	0.99963343	0.71000000	0.01393206	0.30
	SF-CTBS	0.99963343	0.72250000	0.01203568	0.61
	SF-TCIMBS	0.99963343	0.73250000	0.01927175	0.90
	SB-CTBS	0.99963343	0.71250000	0.01168866	27.49
	SB-TCIMBS	0.99969453	0.75750000	0.03766373	44.28
	SB-TCIMBS*	0.99969453	0.72500000	0.01703812	170.59
$\mathbf{p}_4$	**UBS**	0.99957234	0.73250000	0.02601417	0.000566
	SCBS	0.99926686	0.77500000	0.01692815	0.44
	SF-CTBS	0.99975562	0.75250000	0.01403715	0.61
	SF-TCIMBS	0.99969453	0.74500000	0.01972630	0.90
	SB-CTBS	0.99926686	0.72750000	0.03491447	27.70
	SB-TCIMBS	0.93786657	0.67000000	0.04617791	44.25
	SB-TCIMBS*	0.99975562	0.75250000	0.01639296	170.58
$\mathbf{p}_5$	**UBS**	0.99960288	0.67250000	0.02501222	0.000566
	SCBS	0.99917522	0.66750000	0.01116813	0.30
	SF-CTBS	0.99951124	0.67000000	0.01240469	0.62
	SF-TCIMBS	0.99963343	0.65500000	0.01698436	0.90
	SB-CTBS	0.99911413	0.71000000	0.02617058	27.53
	SB-TCIMBS	0.99385997	0.73750000	0.10491691	44.17
	SB-TCIMBS*	0.99969453	0.67500000	0.01524682	167.16

TABLE XII

BAND SET SELECTED BY UBS, CSCBS, AND TCIMBS ON DETECTION OF FULL TARGETS $\mathbf{D} = [\mathbf{p}_1, \mathbf{p}_2, \mathbf{p}_3, \mathbf{p}_4, \mathbf{p}_5]$

UBS	1	10	20	29	39	48	57	67	76	86	95	104	114	123	132	142	151	161
CSCBS-SFBS	122	128	127	154	51	50	133	136	49	27	134	142	121	14	55	132	129	149
SF-TCIMBS	122	128	71	45	52	73	18	47	155	135	142	133	49	149	129	57	161	132
CSCBS-SBBS	122	142	143	69	133	129	49	135	134	132	70	108	124	111	112	110	131	56
SB-TCIMBS	122	142	143	69	129	133	49	135	134	132	70	108	131	124	56	121	137	111
SB-TCIMBS*	14	29	41	49	51	65	69	84	93	95	108	111	122	129	133	134	142	153

TABLE XIII

AUC VALUES OF (P_D, P_F), (P_D, τ), AND (P_F, τ) CALCULATED FROM THE RESULTS IN FIG. 9 AND RUNNING TIME OF EACH BS METHOD

Method	AUC of (P_D, P_F)	AUC of (P_D, τ)	AUC of (P_F, τ)	Running time (s)
UBS(TCIMF)	0.99781186	0.59657895	0.02902011	0.000566
CSCBS-SFBS	0.99809587	0.58289474	0.01745033	0.81
SF-TCIMBS	0.99810877	0.58815789	0.01894653	1.06
CSCBS-SBBS	0.99466842	0.60236842	0.04683959	28.46
SB-TCIMBS	0.99638537	0.65552632	0.04355040	50.60
SB-TCIMBS*	0.99821205	0.59289474	0.01729826	182.98

TABLE XIV

SAM OF EACH TARGET SIGNATURE FOR HYDICE DATA

SAM	$\mathbf{p}_1$	$\mathbf{p}_2$	$\mathbf{p}_3$	$\mathbf{p}_4$	$\mathbf{p}_5$
$\mathbf{p}_1$	0.0000				
$\mathbf{p}_2$	0.0435	0.0000			
$\mathbf{p}_3$	0.0673	0.0430	0.0000		
$\mathbf{p}_4$	0.1144	0.1479	0.1652	0.0000	
$\mathbf{p}_5$	0.1240	0.1567	0.1710	0.0248	0.0000

especially SB-TCIMBS*, which required the longest time. Similarly, for full multiple-target detection and partial multiple-target detection, Tables IV, VII, IX, XIII, XVI, and XVIII showed that the forward selection method consumed less time than the backward selection method. In particular, since SB-TCIMBS* needed to be implemented L-n_{BS} times to obtain the final band subset, the running time of SB-TCIMBS* was the longest. However, as computing power keeps being improved,

TABLE XV

BAND SET SELECTED BY UBS, CSCBS, AND TCIMBS ON DETECTION OF PARTIAL TARGETS $\mathbf{D} = [\mathbf{p}_1, \mathbf{p}_3, \mathbf{p}_4]$

UBS	1	10	20	29	39	48	57	67	76	86	95	104	114	123	132	142	151	161
CSCBS-SFBS	122	128	127	125	124	138	153	132	126	99	87	69	156	134	5	54	45	53
SF-TCIMBS	122	128	130	140	53	49	126	47	99	169	112	103	97	108	84	156	106	142
CSCBS-SBBS	51	50	49	52	53	54	55	47	48	56	57	45	70	19	90	17	44	15
SB-TCIMBS	45	46	47	44	51	50	52	49	53	54	48	55	56	57	70	69	19	78
SB-TCIMBS*	17	24	27	33	38	42	45	46	50	88	94	106	112	123	144	151	156	159

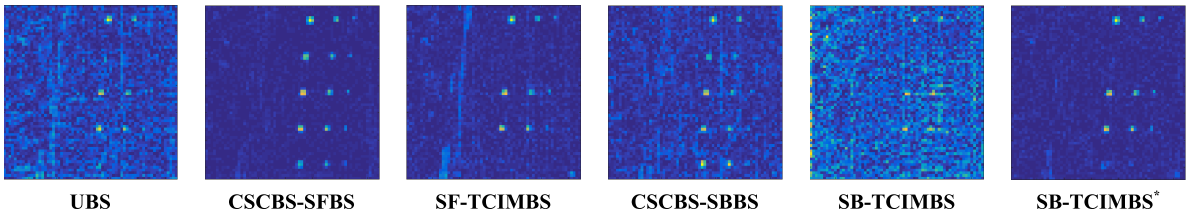

Fig. 10. LCMV detection of partial multiple-target using bands selected by CSCBS and TCIMF detection of partial multiple-target using bands selected by UBS and TCIMBS where partial multiple-target is $\mathbf{D} = [\mathbf{p}_1, \mathbf{p}_3, \mathbf{p}_4]$ in HYDICE data.

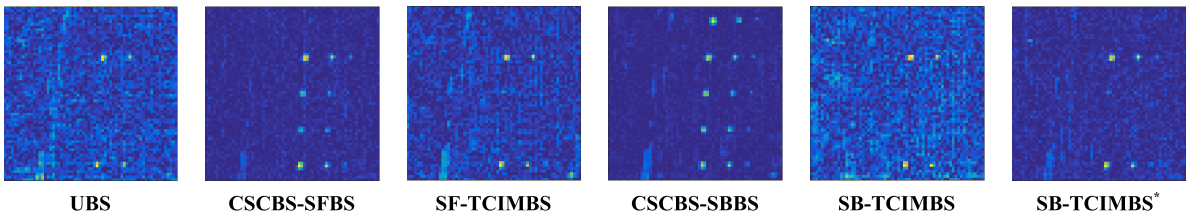

Fig. 11. LCMV detection of partial multiple-target using bands selected by CSCBS and TCIMF detection of partial multiple-target using bands selected by UBS and TCIMBS where partial multiple-target is $\mathbf{D} = [\mathbf{p}_2, \mathbf{p}_5]$ in HYDICE data.

TABLE XVI

AUC VALUES OF (P_D, P_F), (P_D, τ), AND (P_F, τ) CALCULATED FROM THE RESULTS IN FIG. 10 AND RUNNING TIME OF EACH BS METHOD

Method	AUC of (P_D, P_F)	AUC of (P_D, τ)	AUC of (P_F, τ)	Running time (s)
UBS(TCIMF)	0.96769779	0.57409091	0.07840269	0.000566
CSCBS-SFBS	0.99766329	0.59500000	0.02044676	0.88
SF-TCIMBS	0.99820852	0.57954545	0.03195471	0.91
CSCBS-SBBS	0.98366529	0.53500000	0.05492166	31.29
SB-TCIMBS	0.87252698	0.59136364	0.14805508	45.33
SB-TCIMBS*	0.99902081	0.60863636	0.02386903	162.85

TABLE XVII

BAND SET SELECTED BY UBS, CSCBS, AND TCIMBS ON DETECTION OF PARTIAL TARGETS $\mathbf{D} = [\mathbf{p}_2, \mathbf{p}_5]$

UBS	1	10	20	29	39	48	57	67	76	86	95	104	114	123	132	142	151	161
CSCBS-SFBS	122	169	164	133	147	42	129	54	119	113	107	149	25	17	46	49	38	55
SF-TCIMBS	122	118	94	64	120	69	101	162	99	71	131	91	83	113	52	136	45	49
CSCBS-SBBS	143	129	133	142	144	82	83	33	134	46	45	47	44	122	69	123	78	43
SB-TCIMBS	45	46	47	44	43	78	27	28	123	122	69	133	33	134	142	143	129	144
SB-TCIMBS*	27	38	46	49	54	57	61	70	78	82	88	94	107	113	115	122	129	133

TABLE XVIII

AUC VALUES OF (P_D, P_F), (P_D, τ), AND (P_F, τ) CALCULATED FROM THE RESULTS IN FIG. 11 AND RUNNING TIME OF EACH BS METHOD

Method	AUC of (P_D, P_F)	AUC of (P_D, τ)	AUC of (P_F, τ)	Running time (s)
UBS(TCIMF)	0.93750000	0.66125000	0.08369374	0.000566
CSCBS-SFBS	0.99876162	0.67375000	0.02699364	0.87
SF-TCIMBS	0.99695756	0.72375000	0.05995841	1.08
CSCBS-SBBS	0.99678938	0.55625000	0.02439579	31.13
SB-TCIMBS	0.99692698	0.73875000	0.10450342	50.99
SB-TCIMBS*	0.99928143	0.68625000	0.03389922	183.97

the time consumption will become less a problem. In this case, the detection performance will be the main concern.

5) Although this article only investigated the application in target detection, the concepts and ideas derived from TCIMBS can also be applied to other application areas, hyperspectral classification, spectral unmixing, etc., which will be our future work.

X. CONCLUSION

This article develops a new BS method for target detection, TCIMBS. By constraining a target matrix $\mathbf{D}$ of interest and an

undesired target matrix $\mathbf{U}$, TCIMBS minimizes the variance of the desired target signals passing through an FIR filter so as to obtain an optimal band subset that can be used to detect the desired targets in $\mathbf{D}$. Two BP criteria based on TCIMF are designed. In addition, using these two BP criteria, two BS search methods, SF-TCIMBS and SB-TCIMBS along with an improved backward search method, SB-TCIMBS* is also derived as their corresponding counterparts. The experimental results demonstrate the effectiveness of TCIMBS from three aspects. First, unlike UBS, TCIMBS searches for different optimal subsets of bands for different targets. For desired targets, when TCIMF is used to detect the targets on the band subset selected by UBS and TCIMBS, the detection results based on TCIMBS-selected bands perform better than that on UBS-selected bands. Moreover, the band subsets obtained by SF-TCIMBS and SB-TCIMBS* are more capable of suppressing the BKG than UBS. Second, under the same selection mechanism, comparing the single-target-based BS method CTBS, experiments have shown that the bands selected by TCIMBS can effectively reduce the detection of similar undesired targets and also improve the detection performance. Third, since the BKG is complex, the band subset obtained by TCIMBS can effectively reduce the influence of BKG on the detection and optimize the detection results. In general, TCIMBS can effectively select a band subset with strong responsive ability to specific targets in $\mathbf{D}$ and weak response to similar undesired targets in $\mathbf{U}$ while suppressing BKG, which can be successfully applied to the detection of multiple targets of different types. It should be pointed out that this article only investigates target detection as an application to demonstrate the utility of TCIMBS. Its potential can be further explored for other applications such as classification and spectral unmixing.

APPENDIX

Proof of Theorem 1: For simplicity, let $[\mathbf{D}\ \mathbf{U}] = \mathbf{T}$, $[\mathbf{D}\ \mathbf{U}]_{\mathbf{\Omega}_l} = \mathbf{T}_l$, $[\mathbf{D}\ \mathbf{U}]_{\mathbf{\Omega}_{l+1}} = \mathbf{T}_{l+1}$, $\mathbf{c} = \begin{bmatrix} \mathbf{1}_{p*1} \\ \mathbf{0}_{q*1} \end{bmatrix}$, and represent a band image $\mathbf{B}_l$ as a band vector $\mathbf{b}_l$, i.e., $\mathbf{B}_l = \mathbf{b}_l$. Also, let

$$\mathbf{X}_l = \left[\mathbf{r}_l^1, \mathbf{r}_l^2, \ldots, \mathbf{r}_l^N\right] = \begin{bmatrix} r_1^1 & r_1^2 & \cdots & r_1^N \\ r_2^1 & r_2^2 & \cdots & r_2^N \\ \vdots & \vdots & \ddots & \vdots \\ r_l^1 & r_l^2 & \cdots & r_l^N \end{bmatrix} \tag{A1}$$

denote the data matrix using the first l bands, which is an $l \times N$-dimensional matrix, where $\mathbf{r}_l^i = (r_1^i, r_2^i, \ldots, r_l^i)^T$ is the ith sample vector with the first l bands. Then, from (A1), the data matrix $\mathbf{X}_{l+1}$ using $(l+1)$ bands is given by

$$\mathbf{X}_{l+1} = \begin{bmatrix} \mathbf{X}_l \\ \mathbf{r}_{l+1}^T \end{bmatrix} = \begin{bmatrix} r_1^1 & r_1^2 & \cdots & r_1^N \\ r_2^1 & r_2^2 & \cdots & r_2^N \\ \vdots & \vdots & \ddots & \vdots \\ r_l^1 & r_l^2 & \cdots & r_l^N \\ r_{l+1}^1 & r_{l+1}^2 & \cdots & r_{l+1}^N \end{bmatrix} \tag{A2}$$

where $\mathbf{r}_{l+1} = (r_{l+1}^1, r_{l+1}^2, \ldots, r_{l+1}^N)^T$. Let $\mathbf{R}_{\mathbf{\Omega}_l} = (1/N)\sum_{i=1}^N \mathbf{r}_l^i (\mathbf{r}_l^i)^T = (1/N)\mathbf{X}_l\mathbf{X}_l^T$. We have

$$\begin{aligned} \mathbf{R}_{\mathbf{\Omega}_l \cup \{\mathbf{b}_{l+1}\}} &= \frac{1}{N}\sum_{i=1}^N \left(\mathbf{r}_{l+1}^i (\mathbf{r}_{l+1}^i)^T\right) = \frac{1}{N}\mathbf{X}_{l+1}\mathbf{X}_{l+1}^T \\ &= \frac{1}{N}\begin{bmatrix} \mathbf{X}_l \\ \mathbf{r}_{l+1}^T \end{bmatrix}\begin{bmatrix} \mathbf{X}_l^T & \mathbf{r}_{l+1} \end{bmatrix} = \frac{1}{N}\begin{bmatrix} \mathbf{X}_l\mathbf{X}_l^T & \mathbf{X}_l\mathbf{r}_{l+1} \\ \mathbf{r}_{l+1}^T\mathbf{X}_l^T & \mathbf{r}_{l+1}^T\mathbf{r}_{l+1} \end{bmatrix} \\ &= \begin{bmatrix} \mathbf{R}_{\mathbf{\Omega}_l} & (1/N)\mathbf{X}_l\mathbf{r}_{l+1} \\ (1/N)\mathbf{r}_{l+1}^T\mathbf{X}_l^T & (1/N)\mathbf{r}_{l+1}^T\mathbf{r}_{l+1} \end{bmatrix}. \end{aligned} \tag{A3}$$

Now, in order to take care of the scalar $1/N$ in (A3) to simplify the following mathematical derivations, we define $\tilde{\mathbf{X}}_l = (1/\sqrt{N})\mathbf{X}_l$ and $\tilde{\mathbf{r}}_{l+1} = (1/\sqrt{N})\mathbf{r}_{l+1}$, both of which absorb $1/\sqrt{N}$ into their notations to yield

$$\mathbf{R}_{\mathbf{\Omega}_l} = \frac{1}{N}\sum_{i=1}^N \left(\mathbf{r}_l^i (\mathbf{r}_l^i)^T\right) = \sum_{i=1}^N \left(\tilde{\mathbf{r}}_l^i (\tilde{\mathbf{r}}_l^i)^T\right) = \tilde{\mathbf{X}}_l\tilde{\mathbf{X}}_l^T. \tag{A4}$$

Then, (A3) becomes

$$\mathbf{R}_{\mathbf{\Omega}_l \cup \{\mathbf{b}_{l+1}\}} = \frac{1}{N}\begin{bmatrix} \mathbf{X}_l\mathbf{X}_l^T & \mathbf{X}_l\mathbf{r}_{l+1} \\ \mathbf{r}_{l+1}^T\mathbf{X}_l^T & \mathbf{r}_{l+1}^T\mathbf{r}_{l+1} \end{bmatrix} = \begin{bmatrix} \mathbf{R}_{\mathbf{\Omega}_l} & \tilde{\mathbf{X}}_l\tilde{\mathbf{r}}_{l+1} \\ \tilde{\mathbf{r}}_{l+1}^T\tilde{\mathbf{X}}_l^T & \tilde{\mathbf{r}}_{l+1}^T\tilde{\mathbf{r}}_{l+1} \end{bmatrix}. \tag{A5}$$

Using (A4) and (A5) and the following matrix identity:

$$\begin{bmatrix} \mathbf{A}^T\mathbf{A} & \mathbf{A}^T\mathbf{z} \\ \mathbf{z}^T\mathbf{A} & \mathbf{z}^T\mathbf{z} \end{bmatrix}^{-1} = \begin{bmatrix} (\mathbf{A}^T\mathbf{A})^{-1} + \beta\mathbf{A}^\#\mathbf{z}\mathbf{z}^T(\mathbf{A}^\#)^T & -\beta\mathbf{A}^\#\mathbf{z} \\ -\beta\mathbf{z}^T(\mathbf{A}^\#)^T & \beta \end{bmatrix} \tag{A6}$$

with $\mathbf{A} = \tilde{\mathbf{X}}_l^T$ and $\mathbf{z} = \tilde{\mathbf{r}}_{l+1}$, we can further derive

$$\begin{aligned} \mathbf{R}^{-1}_{\mathbf{\Omega}_l \cup \{\mathbf{b}_{l+1}\}} &= \begin{bmatrix} \mathbf{R}_{\mathbf{\Omega}_l} & \tilde{\mathbf{X}}_l\tilde{\mathbf{r}}_{l+1} \\ \tilde{\mathbf{r}}_{l+1}^T\tilde{\mathbf{X}}_l^T & \tilde{\mathbf{r}}_{l+1}^T\tilde{\mathbf{r}}_{l+1} \end{bmatrix}^{-1} \\ &= \begin{bmatrix} \mathbf{R}_{\mathbf{\Omega}_l}^{-1} + \beta\left(\tilde{\mathbf{X}}_l^T\right)^\#\tilde{\mathbf{r}}_{l+1}\tilde{\mathbf{r}}_{l+1}^T\tilde{\mathbf{X}}_l^\# & \left(\tilde{\mathbf{X}}_l^T\right)^\#\tilde{\mathbf{r}}_{l+1} \\ \tilde{\mathbf{r}}_{l+1}^T\tilde{\mathbf{X}}_l^\# & \beta \end{bmatrix} \end{aligned} \tag{A7}$$

where $(\tilde{\mathbf{X}}_l^T)^\# = (\tilde{\mathbf{X}}_l\tilde{\mathbf{X}}_l^T)^{-1}\tilde{\mathbf{X}}_l^T$ and $\beta = \{\tilde{\mathbf{r}}_{l+1}^T[\mathbf{I} - \tilde{\mathbf{X}}_l^T(\tilde{\mathbf{X}}_l^T)^\#]\tilde{\mathbf{r}}_{l+1}\}^{-1} = (\tilde{\mathbf{r}}_{l+1}^T P_{\tilde{\mathbf{X}}_l^T}^\perp \tilde{\mathbf{r}}_{l+1})^{-1}$ due to the fact $P_{\tilde{\mathbf{X}}_l^T}^\perp = \mathbf{I} - \tilde{\mathbf{X}}_l^T(\tilde{\mathbf{X}}_l^T)^\#$ is idempotent, i.e., $(P_{\tilde{\mathbf{X}}_l^T}^\perp)^2 = P_{\tilde{\mathbf{X}}_l^T}^\perp$.

Using (A7) and letting $[\mathbf{D}\ \mathbf{U}]_{\mathbf{\Omega}_l \cup \{\mathbf{b}_{l+1}\}} = \begin{bmatrix} \mathbf{D}_l & \mathbf{U}_l \\ \mathbf{d}_{l+1}^T & \mathbf{u}_{l+1}^T \end{bmatrix}$ where $\mathbf{d}_{l+1} = (d_{l+1}^1, d_{l+1}^2, \ldots, d_{l+1}^p)^T$, $\mathbf{u}_{l+1} = (u_{l+1}^1, u_{l+1}^2, \ldots, u_{l+1}^q)^T$, and $\mathbf{T} = [\mathbf{D}\ \mathbf{U}]$, $\mathbf{t}_{l+1} = (d_{l+1}^1, d_{l+1}^2, \ldots, d_{l+1}^p, u_{l+1}^1, u_{l+1}^2, \ldots, u_{l+1}^q)^T$, we can derive

$$\begin{aligned} &[\mathbf{D}\ \mathbf{U}]^T_{\mathbf{\Omega}_l \cup \{\mathbf{b}_{l+1}\}}\mathbf{R}^{-1}_{\mathbf{\Omega}_l \cup \{\mathbf{b}_{l+1}\}}[\mathbf{D}\ \mathbf{U}]_{\mathbf{\Omega}_l \cup \{\mathbf{b}_{l+1}\}} \\ &= \mathbf{T}^T_{\mathbf{\Omega}_l \cup \{\mathbf{b}_{l+1}\}}\mathbf{R}^{-1}_{\mathbf{\Omega}_l \cup \{\mathbf{b}_{l+1}\}}\mathbf{T}_{\mathbf{\Omega}_l \cup \{\mathbf{b}_{l+1}\}} \\ &= \begin{bmatrix} \mathbf{T}_l^T & \mathbf{t}_{l+1} \end{bmatrix}\begin{bmatrix} \mathbf{R}_{\mathbf{\Omega}_l}^{-1} + \beta\left(\tilde{\mathbf{X}}_l^T\right)^\#\tilde{\mathbf{r}}_{l+1}\tilde{\mathbf{r}}_{l+1}^T\tilde{\mathbf{X}}_l^\# & -\beta\left(\tilde{\mathbf{X}}_l^T\right)^\#\tilde{\mathbf{r}}_{l+1} \\ -\beta\tilde{\mathbf{r}}_{l+1}^T\tilde{\mathbf{X}}_l^\# & \beta \end{bmatrix}\begin{bmatrix} \mathbf{T}_l \\ \mathbf{t}_{l+1}^T \end{bmatrix} \\ &= \mathbf{T}_l^T\left(\mathbf{R}_{\mathbf{\Omega}_l}^{-1} + \beta\left(\tilde{\mathbf{X}}_l^T\right)^\#\tilde{\mathbf{r}}_{l+1}\tilde{\mathbf{r}}_{l+1}^T\tilde{\mathbf{X}}_l^\#\right)\mathbf{T}_l - \beta\mathbf{t}_{l+1}\tilde{\mathbf{r}}_{l+1}^T\tilde{\mathbf{X}}_l^\#\mathbf{T}_l \\ &\quad -\beta\mathbf{T}_l^T\left(\tilde{\mathbf{X}}_l^T\right)^\#\tilde{\mathbf{r}}_{l+1}\mathbf{t}_{l+1}^T + \beta\mathbf{t}_{l+1}\mathbf{t}_{l+1}^T \\ &= \mathbf{T}_l^T\mathbf{R}_{\mathbf{\Omega}_l}^{-1}\mathbf{T}_l + \beta\mathbf{T}_l^T\left(\tilde{\mathbf{X}}_l^T\right)^\#\tilde{\mathbf{r}}_{l+1}\tilde{\mathbf{r}}_{l+1}^T\tilde{\mathbf{X}}_l^\#\mathbf{T}_l \\ &\quad -2\beta\mathbf{t}_{l+1}\tilde{\mathbf{r}}_{l+1}^T\tilde{\mathbf{X}}_l^\#\mathbf{T}_l + \beta\mathbf{t}_{l+1}\mathbf{t}_{l+1}^T \end{aligned}$$

$$
\begin{aligned}
&[\mathbf{D}\ \mathbf{U}]^T_{\mathbf{\Omega}_l\cup\{\mathbf{b}_{l+1}\}}\mathbf{R}^{-1}_{\mathbf{\Omega}_l\cup\{\mathbf{b}_{l+1}\}}[\mathbf{D}\ \mathbf{U}]_{\mathbf{\Omega}_l\cup\{\mathbf{b}_{l+1}\}}\\
&\quad=\mathbf{T}^T_{\mathbf{\Omega}_l\cup\{\mathbf{b}_{l+1}\}}\mathbf{R}^{-1}_{\mathbf{\Omega}_l\cup\{\mathbf{b}_{l+1}\}}\mathbf{T}_{\mathbf{\Omega}_l\cup\{\mathbf{b}_{l+1}\}}\\
&\quad=\left(\mathbf{T}_l^T\mathbf{R}^{-1}_{\mathbf{\Omega}_l}\mathbf{T}_l\right)^{-1}-\frac{\beta\left(\mathbf{T}_l^T\mathbf{R}^{-1}_{\mathbf{\Omega}_l}\mathbf{T}_l\right)^{-1}\left[\mathbf{T}_l^T\left(\tilde{\mathbf{X}}_l^T\right)^{\#}\tilde{\mathbf{r}}_{l+1}-\mathbf{t}_{l+1}\right]\left[\mathbf{T}_l^T\left(\tilde{\mathbf{X}}_l^T\right)^{\#}\tilde{\mathbf{r}}_{l+1}-\mathbf{t}_{l+1}\right]^T\left(\mathbf{T}_l^T\mathbf{R}^{-1}_{\mathbf{\Omega}_l}\mathbf{T}_l\right)^{-1}}{1+\beta\left[\mathbf{T}_l^T\left(\tilde{\mathbf{X}}_l^T\right)^{\#}\tilde{\mathbf{r}}_{l+1}-\mathbf{t}_{l+1}\right]^T\left(\mathbf{T}_l^T\mathbf{R}^{-1}_{\mathbf{\Omega}_l}\mathbf{T}_l\right)^{-1}\left[\mathbf{T}_l^T\left(\tilde{\mathbf{X}}_l^T\right)^{\#}\tilde{\mathbf{r}}_{l+1}-\mathbf{t}_{l+1}\right]}.
\end{aligned}
\tag{A10}
$$

$$
\begin{aligned}
&\mathbf{c}^T\left\{[\mathbf{D}\ \mathbf{U}]^T_{\mathbf{\Omega}_l\cup\{\mathbf{b}_{l+1}\}}\mathbf{R}^{-1}_{\mathbf{\Omega}_l\cup\{\mathbf{b}_{l+1}\}}[\mathbf{D}\ \mathbf{U}]_{\mathbf{\Omega}_l\cup\{\mathbf{b}_{l+1}\}}\right\}\mathbf{c}\\
&\quad=\mathbf{c}^T\left\{\mathbf{T}^T_{\mathbf{\Omega}_l\cup\{\mathbf{b}_{l+1}\}}\mathbf{R}^{-1}_{\mathbf{\Omega}_l\cup\{\mathbf{b}_{l+1}\}}\mathbf{T}_{\mathbf{\Omega}_l\cup\{\mathbf{b}_{l+1}\}}\right\}\mathbf{c}\\
&\quad=\mathbf{c}^T\left(\mathbf{T}_l^T\mathbf{R}^{-1}_{\mathbf{\Omega}_l}\mathbf{T}_l\right)^{-1}\mathbf{c}-\frac{\beta\mathbf{c}^T\left(\mathbf{T}_l^T\mathbf{R}^{-1}_{\mathbf{\Omega}_l}\mathbf{T}_l\right)^{-1}\left[\mathbf{T}_l^T\left(\tilde{\mathbf{X}}_l^T\right)^{\#}\tilde{\mathbf{r}}_{l+1}-\mathbf{t}_{l+1}\right]\left[\mathbf{T}_l^T\left(\tilde{\mathbf{X}}_l^T\right)^{\#}\tilde{\mathbf{r}}_{l+1}-\mathbf{t}_{l+1}\right]^T\left(\mathbf{T}_l^T\mathbf{R}^{-1}_{\mathbf{\Omega}_l}\mathbf{T}_l\right)^{-1}\mathbf{c}}{1+\beta\left[\mathbf{T}_l^T\left(\tilde{\mathbf{X}}_l^T\right)^{\#}\tilde{\mathbf{r}}_{l+1}-\mathbf{t}_{l+1}\right]^T\left(\mathbf{T}_l^T\mathbf{R}^{-1}_{\mathbf{\Omega}_l}\mathbf{T}_l\right)^{-1}\left[\mathbf{T}_l^T\left(\tilde{\mathbf{X}}_l^T\right)^{\#}\tilde{\mathbf{r}}_{l+1}-\mathbf{t}_{l+1}\right]}.
\end{aligned}
\tag{A11}
$$

$$
\begin{aligned}
&=\mathbf{T}_l^T\mathbf{R}^{-1}_{\mathbf{\Omega}_l}\mathbf{T}_l+\beta\left\{\left[\mathbf{T}_l^T\left(\tilde{\mathbf{X}}_l^T\right)^{\#}\tilde{\mathbf{r}}_{l+1}\right]\left[\mathbf{T}_l^T\left(\tilde{\mathbf{X}}_l^T\right)^{\#}\tilde{\mathbf{r}}_{l+1}\right]^T\right.\\
&\qquad\left.-2\mathbf{t}_{l+1}\left[\mathbf{T}_l^T\left(\tilde{\mathbf{X}}_l^T\right)^{\#}\tilde{\mathbf{r}}_{l+1}\right]+\mathbf{t}_{l+1}\mathbf{t}_{l+1}^T\right\}\\
&=\mathbf{T}_l^T\mathbf{R}^{-1}_{\mathbf{\Omega}_l}\mathbf{T}_l+\beta\left[\mathbf{T}_l^T(\tilde{\mathbf{X}}_l^T)^{\#}\tilde{\mathbf{r}}_{l+1}-\mathbf{t}_{l+1}\right]\\
&\quad\times\left[\mathbf{T}_l^T(\tilde{\mathbf{X}}_l^T)^{\#}\tilde{\mathbf{r}}_{l+1}-\mathbf{t}_{l+1}\right]^T
\end{aligned}
\tag{A8}
$$

where $\beta=(\mathbf{t}_{l+1}^TP_{\tilde{\mathbf{X}}_l^T}^{\perp}\mathbf{t}_{l+1})^{-1}$. Using Woodbury's identity

$$
\left[\mathbf{A}+\mathbf{u}\mathbf{v}^T\right]^{-1}=\mathbf{A}^{-1}-\frac{\left[\mathbf{A}^{-1}\mathbf{u}\right]\left[\mathbf{v}^T\mathbf{A}^{-1}\right]}{1+\mathbf{v}^T\mathbf{A}^{-1}\mathbf{u}}
\tag{A9}
$$

with $\mathbf{A}=\mathbf{T}_l^T\mathbf{R}^{-1}_{\mathbf{\Omega}l}\mathbf{T}_l$, $\mathbf{u}=\mathbf{v}=\sqrt{\beta}[\mathbf{T}_l^T(\tilde{\mathbf{X}}_l^T)^{\#}\tilde{\mathbf{r}}_{l+1}-\mathbf{t}_{l+1}]$, we can derive, (A10), as shown at the top of the page. So, (A11), as shown at the top of the page

Since $\beta>0$

$$
\begin{aligned}
&\mathbf{c}^T\left(\mathbf{T}_l^T\mathbf{R}^{-1}_{\mathbf{\Omega}_l}\mathbf{T}_l\right)^{-1}\left[\mathbf{T}_l^T\left(\tilde{\mathbf{X}}_l^T\right)^{\#}\tilde{\mathbf{r}}_{l+1}-\mathbf{t}_{l+1}\right]\\
&\qquad\times\left[\mathbf{T}_l^T\left(\tilde{\mathbf{X}}_l^T\right)^{\#}\tilde{\mathbf{r}}_{l+1}-\mathbf{t}_{l+1}\right]^T\left(\mathbf{T}_l^T\mathbf{R}^{-1}_{\mathbf{\Omega}_l}\mathbf{T}_l\right)^{-1}\mathbf{c}\\
&\quad=\left\|\mathbf{c}^T\left(\mathbf{T}_l^T\mathbf{R}^{-1}_{\mathbf{\Omega}_l}\mathbf{T}_l\right)^{-1}\left[\mathbf{T}_l^T\left(\tilde{\mathbf{X}}_l^T\right)^{\#}\tilde{\mathbf{r}}_{l+1}-\mathbf{t}_{l+1}\right]\right\|^2>0
\end{aligned}
\tag{A12}
$$

and

$$
\begin{aligned}
&\left[\mathbf{T}_l^T\left(\tilde{\mathbf{X}}_l^T\right)^{\#}\tilde{\mathbf{r}}_{l+1}-\mathbf{t}_{l+1}\right]^T\left(\mathbf{T}_l^T\mathbf{R}^{-1}_{\mathbf{\Omega}_l}\mathbf{T}_l\right)^{-1}\left[\mathbf{T}_l^T\left(\tilde{\mathbf{X}}_l^T\right)^{\#}\tilde{\mathbf{r}}_{l+1}-\mathbf{t}_{l+1}\right]\\
&\quad=\left\|\left[\mathbf{T}_l^T\left(\tilde{\mathbf{X}}_l^T\right)^{\#}\tilde{\mathbf{r}}_{l+1}-\mathbf{t}_{l+1}\right]^T\left(\mathbf{T}_l^T\mathbf{R}^{-1}_{\mathbf{\Omega}_l}\mathbf{T}_l\right)^{-1/2}\right\|^2>0.
\end{aligned}
\tag{A13}
$$

Substituting (A13) and (A12) into (A11) yields (A14) as follows:

$$
\begin{aligned}
&\mathbf{c}^T\left\{[\mathbf{D}\ \mathbf{U}]^T_{\mathbf{\Omega}_{l+1}}\mathbf{R}^{-1}_{\mathbf{\Omega}_{l+1}}[\mathbf{D}\ \mathbf{U}]_{\mathbf{\Omega}_{l+1}}\right\}\mathbf{c}-\mathbf{c}^T\left\{[\mathbf{D}\ \mathbf{U}]^T_{\mathbf{\Omega}_l}\mathbf{R}^{-1}_{\mathbf{\Omega}_l}[\mathbf{D}\ \mathbf{U}]_{\mathbf{\Omega}_l}\right\}\mathbf{c}\\
&\quad=\mathbf{c}^T\left\{\mathrm{T}^T_{\mathbf{\Omega}_{l+1}}\mathbf{R}^{-1}_{\mathbf{\Omega}_{l+1}}\mathrm{T}_{\mathbf{\Omega}_{l+1}}\right\}\mathbf{c}-\mathbf{c}^T\left\{\mathrm{T}^T_{\mathbf{\Omega}_l}\mathbf{R}^{-1}_{\mathbf{\Omega}_l}\mathrm{T}_{\mathbf{\Omega}_l}\right\}\mathbf{c}\\
&\quad=-\frac{\beta\left\|\mathbf{c}^T\left(\mathrm{T}_l^T\mathbf{R}^{-1}_{\mathbf{\Omega}_l}\mathrm{T}_l\right)^{-1}\left[\mathrm{T}_l^T(\tilde{\mathbf{X}}_l^T)^{\#}\tilde{\mathbf{r}}_{l+1}-\mathbf{t}_{l+1}\right]\right\|^2}{1+\beta\left\|\left[\mathrm{T}_l^T(\tilde{\mathbf{X}}_l^T)^{\#}\tilde{\mathbf{r}}_{l+1}-\mathbf{t}_{l+1}\right]^T\left(\mathrm{T}_l^T\mathbf{R}^{-1}_{\mathbf{\Omega}_l}\mathrm{T}_l\right)^{-1/2}\right\|^2}<0.
\end{aligned}
\tag{A14}
$$

Therefore, $\mathbf{c}^T([\mathbf{D}\ \ \mathbf{U}]^T_{\mathbf{\Omega}_{l+1}}\mathbf{R}^{-1}_{\mathbf{\Omega}_{l+1}}[\mathbf{D}\ \ \mathbf{U}]_{\mathbf{\Omega}_{l+1}})^{-1}\mathbf{c}<\mathbf{c}^T([\mathbf{D}\ \ \mathbf{U}]^T_{\mathbf{\Omega}_l}\mathbf{R}^{-1}_{\mathbf{\Omega}_l}[\mathbf{D}\ \ \mathbf{U}]_{\mathbf{\Omega}_l})^{-1}\mathbf{c}$ is monotonically decreasing. Theorem is proved.

ACKNOWLEDGMENT

The authors would like to thank Prof. X. Geng for his kindness of sharing his codes of sparse constrained band selection (SCBS) used in our experiments.

REFERENCES

[1] A. F. H. Goetz, G. Vane, J. E. Solomon, and B. N. Rock, "Imaging spectrometry for earth remote sensing," *Science*, vol. 228, no. 4704, pp. 1147–1153, Jun. 1985.

[2] R. O. Green *et al.*, "Imaging spectroscopy and the airborne visible/infrared imaging spectrometer," *Remote Sens. Environ.*, vol. 65, no. 3, pp. 227–248, Sep. 1998.

[3] J. M. Bioucas-Dias, A. Plaza, G. Camps-Valls, P. Scheunders, N. Nasrabadi, and J. Chanussot, "Hyperspectral remote sensing data analysis and future challenges," *IEEE Geosci. Remote Sens. Mag.*, vol. 1, no. 2, pp. 6–36, Jun. 2013.

[4] G. Shaw and D. Manolakis, "Signal processing for hyperspectral image exploitation," *IEEE Signal Process. Mag.*, vol. 19, no. 1, pp. 12–16, Jan. 2002.

[5] D. Landgrebe, "Hyperspectral image data analysis," *IEEE Signal Process. Mag.*, vol. 19, no. 1, pp. 17–28, Jan. 2002.

[6] A. Plaza *et al.*, "Recent advances in techniques for hyperspectral image processing," *Remote Sens. Environ.*, vol. 113, pp. S110–S122, Sep. 2009.

[7] C.-I Chang, *Hyperspectral Data Processing: Algorithm Design and Analysis*. New York, NY, USA: Wiley, 2013.

[8] C.-I Chang, *Real-Time Recursive Hyperspectral Sample and Band Processing: Algorithm Architecture and Implementation*. Berlin, Germany: Springer, 2017.

[9] J. Wang and C.-I Chang, "Independent component analysis-based dimensionality reduction with applications in hyperspectral image analysis," *IEEE Trans. Geosci. Remote Sens.*, vol. 44, no. 6, pp. 1586–1600, Jun. 2006.

[10] C.-I Chang and D. Heinz, "Constrained subpixel detection for remotely sensed images," *IEEE Trans. Geosci. Remote Sens.*, vol. 38, no. 3, pp. 1144–1159, May 2000.

[11] D. Manolakis and G. Shaw, "Detection algorithms for hyperspectral imaging applications," *IEEE Signal Process. Mag.*, vol. 19, no. 1, pp. 29–43, Jan. 2002.

[12] J. C. Harsanyi and C.-I Chang, "Hyperspectral image classification and dimensionality reduction: An orthogonal subspace projection approach," *IEEE Trans. Geosci. Remote Sens.*, vol. 32, no. 4, pp. 779–785, Jul. 1994.

[13] X. Geng, K. Sun, L. Ji, H. Tang, and Y. Zhao, "Joint skewness and its application in unsupervised band selection for small target detection," *Sci. Rep.*, vol. 5, no. 1, p. 9915, Apr. 2015.
[14] H. Yu, X. Shang, X. Zhang, L. Gao, M. Song, and J. Hu, "Hyperspectral image classification based on adjacent constraint representation," *IEEE Geosci. Remote Sens. Lett.*, early access, Apr. 9, 2020, doi: 10.1109/LGRS.2020.2982706.
[15] C.-I Chang and S.-S. Chiang, "Anomaly detection and classification for hyperspectral imagery," *IEEE Trans. Geosci. Remote Sens.*, vol. 40, no. 6, pp. 1314–1325, Jun. 2002.
[16] A. Zare and K. C. Ho, "Endmember variability in hyperspectral analysis: Addressing spectral variability during spectral unmixing," *IEEE Signal Process. Mag.*, vol. 31, no. 1, pp. 95–104, Jan. 2014.
[17] J. M. P. Nascimento and J. M. B. Dias, "Vertex component analysis: A fast algorithm to unmix hyperspectral data," *IEEE Trans. Geosci. Remote Sens.*, vol. 43, no. 4, pp. 898–910, Apr. 2005.
[18] L. Miao and H. Qi, "Endmember extraction from highly mixed data using minimum volume constrained nonnegative matrix factorization," *IEEE Trans. Geosci. Remote Sens.*, vol. 45, no. 3, pp. 765–777, Mar. 2007.
[19] S. Zhang, J. Li, H.-C. Li, C. Deng, and A. Plaza, "Spectral–spatial weighted sparse regression for hyperspectral image unmixing," *IEEE Trans. Geosci. Remote Sens.*, vol. 56, no. 6, pp. 3265–3276, Jun. 2018.
[20] D. A. Landgrebe, *Signal Theory Methods in Multispectral Remote Sensing*. New York, NY, USA: Wiley, 2003.
[21] W. Zhang, X. Li, and L. Zhao, "Band priority index: A feature selection framework for hyperspectral imagery," *Remote Sens.*, vol. 10, no. 7, p. 1095, Jul. 2018.
[22] B. Guo, S. R. Gunn, R. I. Damper, and J. D. B. Nelson, "Band selection for hyperspectral image classification using mutual information," *IEEE Geosci. Remote Sens. Lett.*, vol. 3, no. 4, pp. 522–526, Oct. 2006.
[23] M. Gong, M. Zhang, and Y. Yuan, "Unsupervised band selection based on evolutionary multiobjective optimization for hyperspectral images," *IEEE Trans. Geosci. Remote Sens.*, vol. 54, no. 1, pp. 544–557, Jan. 2016.
[24] A. Fontanella, E. Marenzi, E. Torti, G. Danese, A. Plaza, and F. Leporati, "A suite of parallel algorithms for efficient band selection from hyperspectral images," *J. Real-Time Image Process.*, vol. 15, no. 3, pp. 537–553, Mar. 2018.
[25] C.-I Chang, Q. Du, T.-L. Sun, and M. L. G. Althouse, "A joint band prioritization and band-decorrelation approach to band selection for hyperspectral image classification," *IEEE Trans. Geosci. Remote Sens.*, vol. 37, no. 6, pp. 2631–2641, Nov. 1999.
[26] C.-I Chang and S. Wang, "Constrained band selection for hyperspectral imagery," *IEEE Trans. Geosci. Remote Sens.*, vol. 44, no. 6, pp. 1575–1585, Jun. 2006.
[27] H. Yang, Q. Du, H. Su, and Y. Sheng, "An efficient method for supervised hyperspectral band selection," *IEEE Geosci. Remote Sens. Lett.*, vol. 8, no. 1, pp. 138–142, Jan. 2011.
[28] Q. Wang, F. Zhang, and X. Li, "Optimal clustering framework for hyperspectral band selection," *IEEE Trans. Geosci. Remote Sens.*, vol. 56, no. 10, pp. 5910–5922, Oct. 2018.
[29] Y. Yuan, J. Lin, and Q. Wang, "Dual-Clustering-Based hyperspectral band selection by contextual analysis," *IEEE Trans. Geosci. Remote Sens.*, vol. 54, no. 3, pp. 1431–1445, Mar. 2016.
[30] S. Jia, G. Tang, J. Zhu, and Q. Li, "A novel ranking-based clustering approach for hyperspectral band selection," *IEEE Trans. Geosci. Remote Sens.*, vol. 54, no. 1, pp. 88–102, Jan. 2016.
[31] Y.-L. Chang, B.-F. Shu, T.-J. Hsieh, C.-Y. Chu, and J.-P. Fang, "Band selection for hyperspectral images based on impurity function," in *Proc. IEEE Int. Geosci. Remote Sens. Symp.*, Vancouver, BC, Canada, Jul. 2011, pp. 2369–2372.
[32] Y. Liu, J. Yang, Y. Chen, K. Tan, L. Wang, and X. Yan, "Stability analysis of hyperspectral band selection algorithms based on neighborhood rough set theory for classification," *Chemometric Intell. Lab. Syst.*, vol. 169, pp. 35–44, Oct. 2017.
[33] P. Pudil, J. Novovičová, and J. Kittler, "Floating search methods in feature selection," *Pattern Recognit. Lett.*, vol. 15, no. 11, pp. 1119–1125, Nov. 1994.
[34] M. Zhang, J. Ma, and M. Gong, "Unsupervised hyperspectral band selection by fuzzy clustering with particle swarm optimization," *IEEE Geosci. Remote Sens. Lett.*, vol. 14, no. 5, pp. 773–777, May 2017.
[35] Y. Xu, Q. Du, and N. H. Younan, "Particle swarm optimization-based band selection for hyperspectral target detection," *IEEE Geosci. Remote Sens. Lett.*, vol. 14, no. 4, pp. 554–558, Apr. 2017.
[36] H. Su, B. Yong, and Q. Du, "Hyperspectral band selection using improved firefly algorithm," *IEEE Geosci. Remote Sens. Lett.*, vol. 13, no. 1, pp. 68–72, Jan. 2016.
[37] J. Gao, Q. Du, L. Gao, X. Sun, Y. Wu, and B. Zhang, "Ant colony optimization for supervised and unsupervised hyperspectral band selection," in *Proc. 5th Workshop Hyperspectral Image Signal Process., Evol. Remote Sens. (WHISPERS)*, Gainesville, FL, USA, Jun. 2013, pp. 1–4.
[38] J. Feng, L. C. Jiao, X. Zhang, and T. Sun, "Hyperspectral band selection based on trivariate mutual information and clonal selection," *IEEE Trans. Geosci. Remote Sens.*, vol. 52, no. 7, pp. 4092–4105, Jul. 2014.
[39] Y. Yuan, X. Zheng, and X. Lu, "Discovering diverse subset for unsupervised hyperspectral band selection," *IEEE Trans. Image Process.*, vol. 26, no. 1, pp. 51–64, Jan. 2017.
[40] L. Wang *et al.*, "Band subset selection for anomaly detection in hyperspectral imagery," *IEEE Trans. Geosci. Remote Sens.*, vol. 55, no. 9, pp. 1–12, Jun. 2017.
[41] J. C. Harsanyi, "Detection and classification of subpixel spectral signatures in hyperspectral image sequences," Ph.D. dissertation, Dept. Elect. Eng., Univ. Maryland, Baltimore County, MD, USA, Aug. 1993.
[42] X. Geng, K. Sun, and L. Ji, "Band selection for target detection in hyperspectral imagery using sparse CEM," *Remote Sens. Lett.*, vol. 5, no. 12, pp. 1022–1031, Dec. 2014.
[43] Y. Wang *et al.*, "Constrained-target band selection for multiple-target detection," *IEEE Trans. Geosci. Remote Sens.*, vol. 57, no. 8, pp. 6079–6103, Aug. 2019.
[44] H. Ren and C.-I Chang, "Target-constrained interference-minimized approach to subpixel target detection for hyperspectral imagery," *Opt. Eng.*, vol. 39, no. 12, pp. 3138–3145, Dec. 2000.
[45] Q. Du and C.-I Chang, "A signal-decomposed and interference-annihilated approach to hyperspectral target detection," *IEEE Trans. Geosci. Remote Sens.*, vol. 42, no. 4, pp. 892–906, Apr. 2004.
[46] C. Yu, Y. Wang, M. Song, and C.-I Chang, "Class signature-constrained background-suppressed approach to band selection for classification of hyperspectral images," *IEEE Trans. Geosci. Remote Sens.*, vol. 57, no. 1, pp. 14–31, Jan. 2019.
[47] C.-I Chang, "Statistical detection theory approach to hyperspectral image classification: Performance analysis," *IEEE Trans. Geosci. Remote Sens.*, vol. 57, no. 4, pp. 2057–2074, Apr. 2019.
[48] C.-I Chang and Q. Du, "Estimation of number of spectrally distinct signal sources in hyperspectral imagery," *IEEE Trans. Geosci. Remote Sens.*, vol. 42, no. 3, pp. 608–619, Mar. 2004.
[49] O. L. Frost, "An algorithm for linearly constrained adaptive array processing," *Proc. IEEE*, vol. JPROC-60, no. 8, pp. 926–935, Aug. 1972.
[50] C.-I Chang, "Multiparameter receiver operating characteristic analysis for signal detection and classification," *IEEE Sensors J.*, vol. 10, no. 3, pp. 423–442, Mar. 2010.
[51] M. Song, X. Shang, and C.-I Chang, "3-D receiver operating characteristic analysis for hyperspectral image classification," *IEEE Trans. Geosci. Remote Sens.*, early access, Apr. 29, 2020, doi: 10.1109/TGRS.2020.2987137.
[52] C.-I Chang, H. Ren, Q. Du, S.-S. Chiang, and A. Ifarraguerri, "An ROC analysis for subpixel detection," in *Proc. IEEE Int. Geosci. Remote Sens. Symp.*, Sydney, NSW, Australia, Jul. 2001, pp. 2355–2357.

Xiaodi Shang (Graduate Student Member, IEEE) received the B.S. degree in software engineering from Qingdao University, Qingdao, China, in 2016. She is pursuing the Ph.D. degree in computer application technology with Dalian Maritime University, Dalian, China.

Her research includes hyperspectral image classification, band selection, and applications.

Meiping Song (Member, IEEE) received the Ph.D. degree from the College of Computer Science and Technology, Harbin Engineering University, Harbin, China, in 2006.

From 2013 to 2014, she was a Visiting Associate Research Scholar with Remote Sensing Signal and Image Processing Laboratory, University of Maryland, Baltimore County, Baltimore, MD, USA. She is an Associate Professor with the College of Information Science and Technology, Dalian Maritime University, Dalian, China. Her research includes remote sensing and hyperspectral image processing.

Yulei Wang (Member, IEEE) received the B.S. and Ph.D. degrees in signal and information processing from Harbin Engineering University, Harbin, China, in 2009 and 2015, respectively.

She was awarded by the China Scholarship Council in 2011 as a joint Ph.D. Student to study with the Remote Sensing Signal and Image Processing Laboratory, University of Maryland, Baltimore County, Baltimore, MD, USA. She is a Lecturer with the College of Information Science and Technology, Dalian Maritime University, Dalian, China. Her research interests include hyperspectral image processing and vital sign signal processing.

Chunyan Yu (Member, IEEE) received the B.S. and Ph.D. degrees from Dalian Maritime University, Dalian, China, in 2004 and 2012, respectively.

In 2004, she joined the College of Computer Science and Technology, Dalian Maritime University. From June 2013 to June 2016, she was a Post-Doctoral Fellow with the Information Science and Technology College, Dalian Maritime University. From September 2014 to September 2015, she was a Visiting Scholar with the College of Physicians and Surgeons, Columbia University, New York, NY, USA. She is a Lecturer with the Information Science and Technology College, Dalian Maritime University. Her research interests are image segmentation, hyperspectral image classification, and pattern recognition.

Haoyang Yu (Member, IEEE) received the B.S. degree in information and computing science from Northeastern University, Shenyang, China, in 2013 and the Ph.D. degree in cartography and geographic information system from the Key Laboratory of Digital Earth Science, Aerospace Information Research Institute, Chinese Academy of Sciences (CAS), Beijing, China, in 2019.

He is a Xing Hai Associate Professor with the Center of Hyperspectral Imaging in Remote Sensing (CHIRS), Information Science and Technology College, Dalian Maritime University, Dalian, China. His research focuses on models and algorithms for hyperspectral image processing, analysis, and applications.

Fang Li received the B.S. degree from the College of Information Science and Technology, Qufu Normal University, Rizhao, China, in 2017. She is pursuing the Ph.D. degree in computer application technology with Dalian Maritime University, Dalian, China.

Her research interests include remote sensing and hyperspectral image processing.

Chein-I Chang (Life Fellow, IEEE) received the B.S. degree in mathematics from Soochow University, Taipei, Taiwan, in 1973, the M.S. degree in mathematics from the Institute of Mathematics, National Tsing Hua University, Hsinchu, Taiwan, in 1975, the M.A. degree in mathematics from the State University of New York at Stony Brook, Stony Brook, NY, USA, in 1977, the M.S. and M.S.E.E. degrees from the University of Illinois at Urbana–Champaign, Urbana, IL, USA, in 1982, and the Ph.D. degree in electrical engineering from the University of Maryland, College Park, MD, USA, in 1987.

He has been with the University of Maryland, Baltimore County (UMBC), Baltimore, MD, since 1987, where he is currently a Professor with the Department of Computer Science and Electrical Engineering. He has been holding the Chang Jiang Scholar Chair Professorship and the Director of the Center for Hyperspectral Imaging in Remote Sensing (CHIRS), Dalian Maritime University, Dalian, China, since 2016. He has also been the Chair Professor with National Chiao Tung University, Hsinchu, since 2019. He has authored four books titled *Hyperspectral Imaging: Techniques for Spectral Detection and Classification* (Kluwer Academic Publishers, 2003), *Hyperspectral Data Processing: Algorithm Design and Analysis* (John Wiley & Sons, 2013), *Real Time Progressive Hyperspectral Image Processing: Endmember Finding and Anomaly Detection* (Springer, 2016), and *Recursive Hyperspectral Sample and Band Processing: Algorithm Architecture and Implementation* (Springer, 2017). He has edited two books titled *Recent Advances in Hyperspectral Signal and Image Processing* in 2006 and *Hyperspectral Data Exploitation: Theory and Applications* (John Wiley & Sons, 2007) and co-edited with A. Plaza a book titled *High Performance Computing in Remote Sensing* (CRC Press, 2007). He holds seven patents on hyperspectral image processing. His research interests include multispectral/hyperspectral image processing, automatic target recognition, and medical imaging.

Dr. Chang is a fellow of SPIE. He received the National Research Council Senior Research Associateship Award sponsored by the U.S. Army Soldier and Biological Chemical Command, Edgewood Chemical and Biological Center, Aberdeen Proving Ground, MD, from 2002 to 2003. He was a plenary speaker for the Society for Photo-Optical Instrumentation Engineers (SPIE) Optics+Applications, Remote Sensing Symposium, in 2009. He was a Guest Editor of a special issue of the *Journal of High Speed Networks* on Telemedicine and Applications in April 2000 and a Co-Guest Editor of another special issue of the same journal on Broadband Multimedia Sensor Networks in Healthcare Applications in April 2007. He is also a Co-Guest Editor of special issues on High Performance Computing of Hyperspectral Imaging for the *International Journal of High Performance Computing Applications* in December 2007, Signal Processing and System Design in Health Care Applications for the *EURASIP Journal on Advances in Signal Processing* in 2009, Multipsectral, Hyperspectral, and Polarimetric Imaging Technology for the *Journal of Sensors* in 2016, and Hyperspectral Imaging and Applications for the *Remote Sensing*, in 2018.